

Hsp83/Hsp90 Physically Associates with Insulin Receptor to Promote Neural Stem Cell Reactivation

Jiawen Huang¹ and Hongyan Wang^{1,2,3,*}¹Neuroscience & Behavioural Disorders Programme, Duke-NUS Medical School, 8 College Road, Singapore 169857, Singapore²Department of Physiology, Yong Loo Lin School of Medicine, National University of Singapore, Singapore 117597, Singapore³NUS Graduate School for Integrative Sciences and Engineering, National University of Singapore, 28 Medical Drive, Singapore 117456, Singapore*Correspondence: hongyan.wang@duke-nus.edu.sg<https://doi.org/10.1016/j.stemcr.2018.08.014>

SUMMARY

Neural stem cells (NSCs) have the ability to exit quiescence and reactivate in response to physiological stimuli. In the *Drosophila* brain, insulin receptor (InR)/phosphatidylinositol 3-kinase (PI3K)/Akt pathway triggers NSC reactivation. However, intrinsic mechanisms that control the InR/PI3K/Akt pathway during reactivation remain unknown. Here, we have identified heat shock protein 83 (Hsp83/Hsp90), a molecular chaperone, as an intrinsic regulator of NSC reactivation. Hsp83 is both necessary and sufficient for NSC reactivation by promoting the activation of InR pathway in larval brains in the presence of dietary amino acids. Both Hsp83 and its co-chaperone Cdc37 physically associate with InR. Finally, reactivation defects observed in brains depleted of *hsp83* were rescued by over-activation of the InR/PI3K/Akt pathway, suggesting that Hsp83 functions upstream of the InR/PI3K/Akt pathway during NSC reactivation. Given the conservation of Hsp83 and the InR pathway, our finding may provide insights into the molecular mechanisms underlying mammalian NSC reactivation.

INTRODUCTION

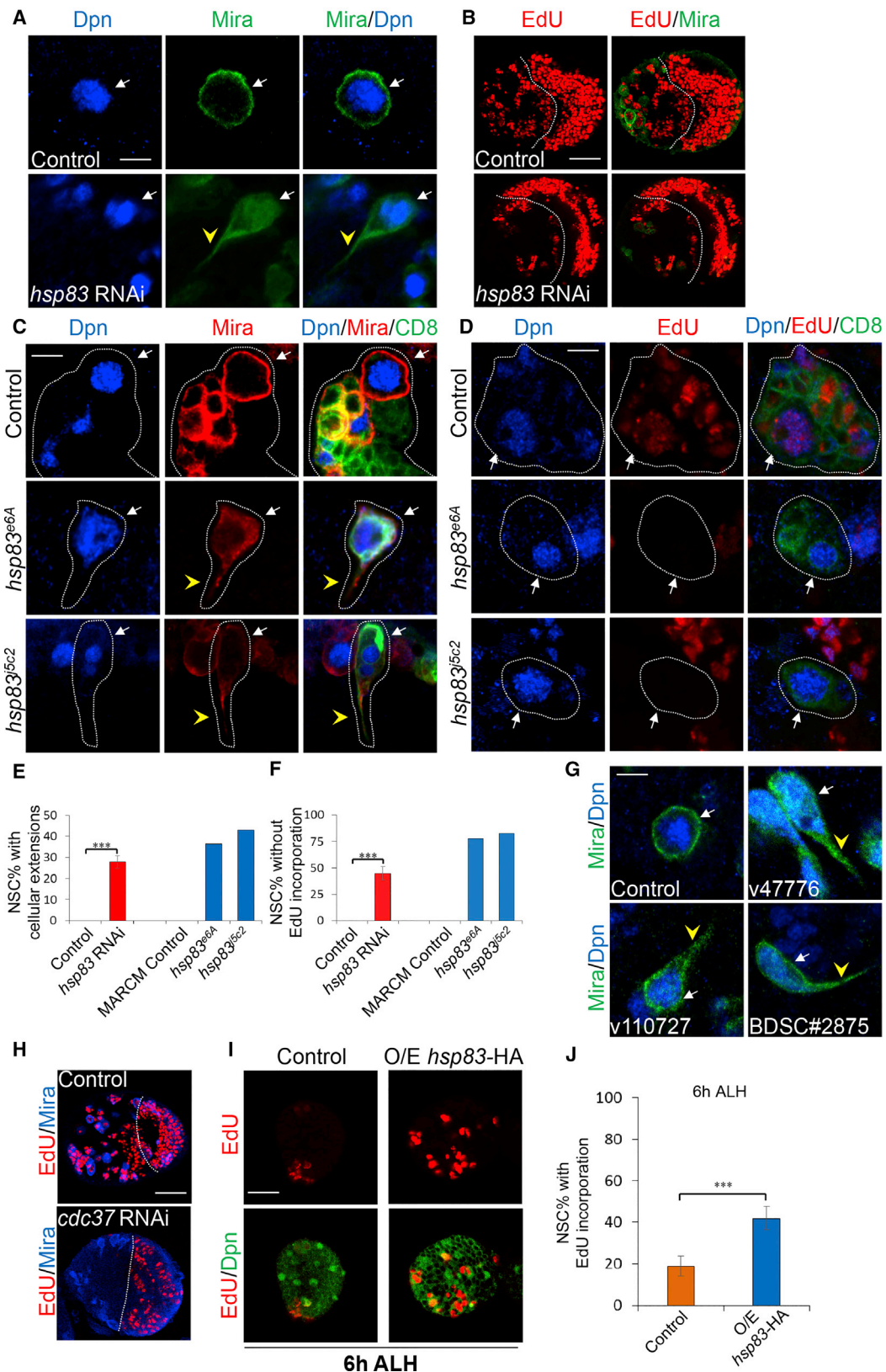
The balance between proliferation and quiescence of stem cells is crucial in maintaining tissue homeostasis. Neural stem cells (NSCs) in the brain have the ability to be reactivated from a reversible quiescent state to generate new neurons. In the mammalian adult brain, the majority of adult NSCs are quiescent and are not actively dividing (Doetsch et al., 1999; Morshead et al., 1994). Interestingly, these quiescent NSCs can be reactivated and participate in neurogenesis upon various extrinsic stimuli (Ahn and Joyner, 2005; Daynac et al., 2013, 2016; Faiz et al., 2015; Kawai et al., 2017; Lugert et al., 2010; Wang et al., 2011). Dysregulation of the balance between proliferation and quiescence of NSCs may contribute to neurodevelopmental disorders such as microcephaly (Baser et al., 2017; Cloetta et al., 2013). Reactivating quiescent NSCs may also provide therapeutic strategies for the treatment of brain injuries or neurodegenerative disorders.

Recently, *Drosophila* NSCs, neuroblasts, have emerged as an excellent *in vivo* model for the study of NSC quiescence and reactivation. NSCs exit the cell cycle, shrink in size, and enter quiescence at the end of embryogenesis under the control of the spatial Hox protein, temporal identity factors, and a homeodomain differentiation factor Prospero (Isshiki et al., 2001; Lai and Doe, 2014; Tsuji et al., 2008). At early larval stages, following 24 hr of quiescence, they are reactivated in response to feeding (Britton and Edgar, 1998; Ito and Hotta, 1992; Truman and Bate, 1988). Dietary amino acids present in the food are sensed by the fat body, which functions equivalent to the

mammalian liver and adipose tissue (Colombani et al., 2003). The fat body generates mitogens, stimulating blood-brain barrier glial cells to secrete insulin-like peptides (dILPs). dILPs act locally by activating the insulin receptor (InR)/phosphatidylinositol 3-kinase (PI3K)/Akt pathway in underlying NSCs and promoting their reactivation (Britton and Edgar, 1998; Chell and Brand, 2010; Sousa-Nunes et al., 2011). Blood-brain barrier glial cells synchronize NSC reactivation via calcium oscillations through gap junctions (Speder and Brand, 2014), while cortex glial cells remodel to promote new-born neuron survival (Speder and Brand, 2018). Besides InR pathway, the spindle matrix complex intrinsically promotes NSC reactivation (Li et al., 2017), while the Hippo pathway maintains NSC quiescence (Ding et al., 2016; Poon et al., 2016). In mammalian brains, insulin-like growth factor-1 (IGF-1) produced by astroglial cells has a similar role in promoting NSC proliferation in response to brain injury (Mairet-Coello et al., 2009; Yan et al., 2006; Ye et al., 2004). In addition, IGF-1 receptor (IGF-1R) promotes the proliferation of mammalian NSCs (Arsenijevic et al., 2001), and human IGF-1R mutations are associated with microcephaly (Juanes et al., 2015), suggesting that the insulin pathway is likely conserved from flies to humans in promoting NSC proliferation. However, how the insulin pathway is regulated during NSC reactivation is still poorly understood.

Here, we show that a highly conserved chaperone, Hsp83/Hsp90, is required for the activation of the InR/PI3K/Akt pathway during NSC reactivation. Hsp83 functions in a wide variety of biological processes, including





(legend on next page)



cell polarity, DNA transcription, and chromatin remodeling (Andersen et al., 2012; Pratt and Toft, 1997; Sawarkar et al., 2012; Tariq et al., 2009). Unlike Hsp70, eukaryotic Hsp83/Hsp90 does not act in nascent protein folding, rather, it binds to substrate proteins that are in a near native state at a late stage of folding (Young et al., 2001). We show that Hsp83 is necessary and sufficient for NSC reactivation in the presence of dietary amino acids. Its co-chaperones Cdc37 and Hsp70 mediate the association between Hsp83 and its client protein kinases and steroid hormone receptors, respectively (Eckl and Richter, 2013; Young et al., 2001). We show that the activation of the InR/PI3K/Akt pathway is dependent on Hsp83 and Cdc37 function in larval brains. Hsp83 and Cdc37 physically associate with InR, but not Akt. Finally, the *hsp83* knockdown phenotype is rescued by over-activation of the InR/PI3K/Akt pathway.

RESULTS

Hsp83 Is Required Intrinsically for NSC Reactivation

To identify regulators of NSC reactivation, we used an NSC-specific driver *insc-GAL4* to perform an unbiased RNAi screening in NSCs. Our screen identified an RNAi line (VDRC no. 108568), which knocks down *hsp83* expression, exhibiting defective NSC reactivation, with cellular extensions, a hallmark of quiescent NSCs, observed in $27.7\% \pm 3.0\%$ (Figures 1A and 1E; $n = 1,452$, 41 brain lobes) of NSCs at 72 hr after larval hatching (ALH) at 29°C . In comparison, all control NSCs were reactivated and lost their cellular extensions at the same stage (Figures 1A and 1E; $n = 1,084$, 20 brain lobes). This finding suggests that these

NSCs failed to be reactivated and remained in a quiescent state upon *hsp83* knockdown. Next, in order to examine if NSCs with *hsp83* knockdown are able to enter the cell cycle, we carried out 5-ethynyl-2'-deoxyuridine (EdU) incorporation experiments. All control NSCs (Figures 1B and 1F; $n = 756$, 20 brain lobes) incorporated EdU at 72 hr ALH at 29°C . By contrast, at the same condition, $44.7\% \pm 6.3\%$ ($n = 824$, 24 brain lobes) of NSCs failed to incorporate EdU with *hsp83* knockdown (Figures 1B and 1F). Next, we examined the phenotype of an amorphic *hsp83^{jsC2}* and hypomorphic *hsp83^{e6A}* in mosaic analysis with a repressible cell marker (MARCM) clones (Lee and Luo, 2001). While all NSCs in wild-type control clones exhibited normal round shapes without any cellular extensions ($n = 58$), 43.0% ($n = 114$) of *hsp83^{jsC2}* NSC clones and 36.4% ($n = 266$) of *hsp83^{e6A}* NSC clones contained NSCs with cellular extensions (Figures 1C and 1E). These observations further show that NSCs remain quiescent after loss of *hsp83*. To examine the proliferative status of the NSCs, we performed EdU pulse-chase analysis. At 96 hr ALH, all NSCs in wild-type control clones were actively dividing evident by EdU incorporation ($n = 101$). Unlike the wild-type control clones, 82.8% ($n = 82$) and 77.9% ($n = 87$) of NSC clones with *hsp83^{jsC2}* and *hsp83^{e6A}*, respectively, failed to incorporate EdU (Figures 1D and 1F). Furthermore, the NSC quiescence phenotype of *hsp83* mutants were fully rescued by introducing a 21.8-kb bacterial artificial chromosome (BAC) CH322-129N17 containing *hsp83* (*hsp83-BAC*). A total of 39.7% ($n = 126$) and 36.4% ($n = 107$) NSCs in *hsp83^{jsC2}* and *hsp83^{e6A}* MARCM clones showed cellular extensions (Figure S1A). However, when *hsp83-BAC* was expressed, none of NSCs in *hsp83^{jsC2}* ($n = 117$) and *hsp83^{e6A}* ($n = 107$) MARCM clones exhibited

Figure 1. Hsp83 and Its Co-chaperone Cdc37 Are Required for NSC Reactivation

(A) Larval NSCs of control (UAS-*dicer2*) and *hsp83* RNAi (VDRC no. 108568) induced with *insc-Gal4* at 72 hr ALH were stained for Deadpan (Dpn) and Miranda (Mira).

(B) Larval brains of control (UAS-*dicer2*) and *hsp83* RNAi (VDRC no. 108568) induced with *insc-Gal4* at 72 hr ALH were labeled with EdU and Mira.

(C) Larval NSC clones of wild-type control, *hsp83^{e6A}* and *hsp83^{jsC2}* at 96 hr ALH were stained for GFP, Dpn, and Mira. NSC lineages were marked with CD8-GFP.

(D) Larval NSC clones of wild-type control, *hsp83^{e6A}*, and *hsp83^{jsC2}* at 96 hr ALH were labeled with GFP, Dpn, and EdU. NSC lineages were marked with CD8-GFP.

(E and F) Quantifications of cellular extensions (E) and EdU incorporation (F) for control, *hsp83* RNAi, MARCM control clone, *hsp83^{e6A}*, and *hsp83^{jsC2}* MARCM clones. Data are presented as mean \pm SD for RNAi knockdown.

(G) Larval NSCs of control (UAS-*dicer2*) and *cdc37* RNAi (VDRC no. 47776/v47776, v110727 and BDSC no. 28756; induced with *insc-Gal4* at 72 hr ALH were stained for Dpn and Mira).

(H) Larval brains of control (UAS-*dicer2*) and *cdc37* RNAi (v47776) induced with *insc-Gal4* at 72 hr ALH were labeled with EdU and Mira.

(I and J) Larval brains of control (UAS-*dicer2*) and UAS-*hsp83-HA* under the control of *insc-Gal4* at 6 hr ALH were labeled with EdU and Dpn. Data are presented in (J) as mean \pm SD.

White arrows point to NSCs and yellow arrowheads point to cellular extensions of NSCs (A, C, D, and G). Central brain is to the left of white dotted lines (B and H). Clone outline is indicated by white dotted lines (C and D). Statistical analyses were done comparing two different genotypes using a two-tailed Student's t test (E, F, and J). *** $p < 0.001$. Scale bars, 5 μm in (A), (C), (D), and (G), 30 μm in (B) and (H), and 15 μm in (I).



cellular extensions (Figure S1A). Similarly, 78.3% (n = 46) and 70.8% (n = 72) NSCs in *hsp83^{isc2}* and *hsp83^{ea}* MARCM clones failed to incorporate with EdU (Figure S1A), while all NSCs from *hsp83^{isc2}* with *hsp83*-BAC (n = 95) and *hsp83^{ea}* with *hsp83*-BAC (n = 70) were incorporated with EdU (Figure S1A). Taken together, these results indicate that Hsp83 is required for NSC reactivation.

We carried out a time course experiment and examined larval brains at 24, 48, and 72 hr ALH. At 24 hr ALH, most control NSCs were reactivated, with only 4.9% ± 1.0% (n = 2,174, 37 brain lobes) showing cellular extensions, suggesting that they were still in quiescence (Figures S1C and S1E). With *hsp83* knockdown under the *insc*-Gal4 driver, 15.4% ± 1.3% (n = 1,535, 28 brain lobes) of NSCs possess cellular extensions at 24 hr ALH (Figures S1C and S1E). Loss of cellular extensions of NSCs seemed to precede cell-cycle re-entry. At 24 hr ALH, 19.5% ± 3.8% (n = 1,205, 22 brain lobes) of control NSCs failed to incorporate EdU (Figures S1B and S1D), while 63.1% ± 5.0% (n = 1,193, 24 brain lobes) NSCs with *hsp83* knockdown were EdU-negative (Figures S1B and S1D). This observation suggests that NSC reactivation is defective when *hsp83* is knocked down at early larval stages. At 48 hr ALH, all control NSCs showed round cell morphology without cellular extension (Figures S1C and S1E; n = 1,625, 30 brain lobes) and nearly all of the NSCs incorporated EdU (Figures S1B and S1D; 98.2% ± 1.4%, n = 704, 21 brain lobes). In comparison, with *hsp83* knockdown, 27.2% ± 2.9% (n = 1,254, 20 brain lobes) of NSCs still showed cellular extensions (Figures S1C and S1E), while 48.7% ± 6.2% (n = 526, 13 brain lobes) of NSCs failed to incorporate EdU (Figures S1B and S1D). At 72 hr ALH, all control NSCs had no cellular extensions (Figures S1C and S1E; n = 1,221, 13 brain lobes) and incorporated EdU (Figures S1B and S1D; n = 322, 6 brain lobes). By contrast, with *hsp83* knockdown 28.2% ± 2.1% (n = 1,003, 11 brain lobes) of NSCs showed cellular extensions (Figures S1C and S1E) and 49.5% ± 7.4% (n = 290, 5 brain lobes) of NSCs lacked EdU incorporation (Figures S1B and S1D). Taken together, Hsp83 is intrinsically required for NSC reactivation.

Upon *hsp83* knockdown at 72 hr ALH, the sizes of NSCs are variable, ranging from 4 to 11 μm, even when they still maintained cellular extensions, a hallmark of quiescent NSCs. At 24 hr ALH, the diameter of control NSCs was 8.7 ± 0.6 μm (n = 121), while NSC diameters were decreased to 6.8 ± 1.3 μm (n = 129) upon *hsp83* knockdown under *insc*-Gal4 (data not shown). At 72 hr ALH, the average NSC diameter upon *hsp83* RNAi knockdown is 8.1 ± 1.8 μm (n = 124), still smaller than control NSCs (10.6 ± 0.7 μm; data not shown). Similarly, at 72 hr ALH the NSC diameters of *hsp83^{ea}* and *hsp83^{isc2}* were 8.1 ± 1.7 μm (n = 121) and 8.2 ± 1.6 μm (n = 118), respectively. These observations suggest that, although NSC reactivation is

dramatically disrupted upon knocking down *hsp83*, cell growth is incompletely blocked, resulting in enlargement of some of the quiescent NSCs. Thus, cell division and cell growth seemed to be partially uncoupled upon failure of NSC reactivation in NSCs upon *hsp83* depletion. Similar uncoupling of cell division and growth were also reported in other mutants defective in NSC reactivation including *chromator*, which appears to function downstream of the InR signaling pathway (Li et al., 2017).

Mushroom body (MB) neuroblasts do not enter quiescence at the end stage of embryogenesis and are capable of dividing in the absence of dietary amino acids throughout larval stages (Ito and Hotta, 1992; Sousa-Nunes et al., 2011; Truman and Bate, 1988). We investigated whether Hsp83 was required for general proliferation of cells, such as MB neuroblasts. At 24 hr ALH, all MB neuroblasts (Dpn⁺), which were surrounded by Dachshund-positive MB neurons, from both control (n = 224) and *hsp83* RNAi (n = 200), were incorporated with EdU (Figure S1F). This result suggests that proliferation of MB neuroblasts is unaffected by *hsp83* RNAi knockdown.

Co-chaperone Cdc37 Is Required for NSC Reactivation

Functioning as a chaperone, Hsp83 has two major classes of clients, steroid hormone receptors and protein kinases, and requires co-chaperones heat shock protein 70 (Hsp70) or cell division cycle 37 (Cdc37), respectively (Eckl and Richter, 2013). To investigate whether steroid hormone receptors or protein kinases are the potential clients of Hsp83 during NSC reactivation, we tested whether Hsp70 or Cdc37 plays any role during NSC reactivation. There are seven isoforms of *hsp70* in *Drosophila* and we acquired 14 RNAi stocks for these isoforms (Table S1) and knocked down these genes in NSCs using *insc*-Gal4. However, knocking down these isoforms of *hsp70* or Hsp70/Hsp90 organizing protein (*hop*), which coordinates the interaction between Hsp70 and Hsp83 by binding to both of them, did not result in any NSC reactivation defect at both 24 and 72 hr ALH (Table S1 and data not shown). By contrast, at 72 hr ALH at 29°C, in *cdc37* RNAi knockdown (VDRC no. 47776) brains, 16.8% ± 2.2% (n = 947, 11 brain lobes) of NSCs showed cellular processes (Figure 1G), and only 1.5% ± 1.4% (n = 1,135, 14 brain lobes) of NSCs were incorporated with EdU (Figure 1H). Similarly, in two other *cdc37* RNAi lines (VDRC no. 110727 and BDSC no. 28756), 16.1% ± 1.2% (n = 1,352, 18 brain lobes) and 19.7% ± 3.3% (n = 1,812, 28 brain lobes) of NSCs showed cellular extensions, respectively (Figure 1G). These observations suggest that Hsp83 likely functions together with its co-chaperone Cdc37 during NSC reactivation. *cdc37^{ea}* is an amorphic allele in which almost the entire coding region of *cdc37* is deleted (Cutforth and Rubin, 1994). In wild-type NSC MARCM clones, all NSCs were devoid of



cellular extensions at 96 hr ALH (Figures S1G and S1H; $n = 50$). By contrast, in *cdc37^{e4D}* MARCM clones, 28.8% ($n = 198$) of NSCs extend cellular processes (Figures S1G and S1H), suggesting that Cdc37 is required for NSC activation. The process phenotype of *cdc37^{e4D}* was fully rescued by introducing a 22.1-kb BAC CH322-35F18 containing *cdc37* (*cdc37*-BAC). A total of 25.9% ($n = 85$) NSCs in *cdc37^{e4D}* MARCM clones showed cellular extensions, while none of the NSCs ($n = 71$) from *cdc37^{e4D}* with *cdc37*-BAC showed cellular extensions (Figures S1G and S1H). Therefore, we conclude that Cdc37 is required for NSC reactivation.

Overexpression of Hsp83 Leads to Premature NSC Reactivation

To test whether Hsp83 overexpression is sufficient to trigger NSC reactivation, we overexpressed *hsp83*-hemagglutinin (HA) (Kuo et al., 2013) in NSCs using *insc*-Gal4 and examined its effect on NSC proliferation at 6 hr ALH. Hsp83-HA is functional, as it largely rescued the NSC quiescence phenotype in *hsp83^{ISC2}* and *hsp83^{e6A}* mutants (data not shown). At 6 hr ALH, most wild-type control NSCs remained in quiescence, as only 18.8% \pm 4.8% of NSCs ($n = 1,907$, 55 brain lobes) incorporated EdU (Figures 1I and 1J). By contrast, upon *hsp83* overexpression, 41.9% \pm 5.5% ($n = 2,211$, 62 brain lobes) of NSCs incorporated EdU (Figures 1I and 1J). This result suggests that Hsp83 overexpression leads to premature NSC reactivation. However, in the absence of dietary amino acids, Hsp83 overexpressing in NSCs was unable to promote NSC reactivation (data not shown), suggesting that Hsp83 overexpression effect is nutrition dependent. Taken together, Hsp83 is both necessary and sufficient for NSC reactivation in the presence of dietary amino acids.

pInR and Akt Levels Are Decreased upon *hsp83* Depletion

Activation of the InR/PI3K/Akt pathway promotes NSC reactivation (Chell and Brand, 2010; Sousa-Nunes et al., 2011). We investigated whether the InR/PI3K/Akt pathway is activated in NSCs with *hsp83* depleted. To this end, we first analyzed the protein levels of Akt in NSCs, a major component of the InR/PI3K/Akt pathway and a protein kinase that triggers NSC reactivation (Shim et al., 2013). In the central brain of wild-type larvae at 72 hr ALH, Akt protein levels were comparable with its levels in the optic lobe (Figure 2A). However, upon *hsp83* knockdown in central brain NSCs by *insc*-Gal4 at 72 hr ALH, Akt protein levels in the central brain decreased significantly, while its levels in the optic lobe remained similar to control (Figure 2A). Likewise, Akt protein levels in the central brain were reduced significantly upon *cdc37* knockdown by RNAi (Figure 2A). These observations suggest that Hsp83 and Cdc37

may be required for the activation of the InR/PI3K/Akt pathway in NSCs. Next, we examined Akt protein levels in whole-brain protein extracts by western blot. *hsp83* knockdown in larval brains was efficient, as Hsp83 protein levels in the whole brain were reduced to 47.3% \pm 6.8% ($n = 3$) in *hsp83* knockdown samples compared with controls (Figures 2B and 2C). Remarkably, Akt protein levels was only 61.7% \pm 5.5% ($n = 3$) in *hsp83* knockdowns compared with wild-type controls (Figures 2B and 2C). Likewise, upon *cdc37* knockdown in NSCs Akt level was reduced to 67.1% \pm 15.8% ($n = 3$), compared with wild-type control (Figures 2B and 2C). These results suggest that the InR/PI3K/Akt pathway is likely impaired upon depletion of either *hsp83* or *cdc37* in NSCs.

We then examined whether the protein levels of phosphorylated insulin receptor (pInR), the activated form of InR, is altered upon *hsp83* or *cdc37* depletion in larval brains. After *hsp83* knockdown in NSCs under *insc*-Gal4 at 72 hr ALH, only 16.5% \pm 9.7% ($n = 3$) of pInR remained compared with wild-type controls (Figures 2D and 2E). Similarly, knockdown of *cdc37* in NSCs resulted in a dramatic reduction of pInR levels with 23.1% \pm 0.6% ($n = 3$) compared with controls (Figures 2D and 2E). The mRNA levels of *InR* or *akt*, were not obviously altered with *hsp83* or *cdc37* RNAi knockdown (Figures S2A and S2B).

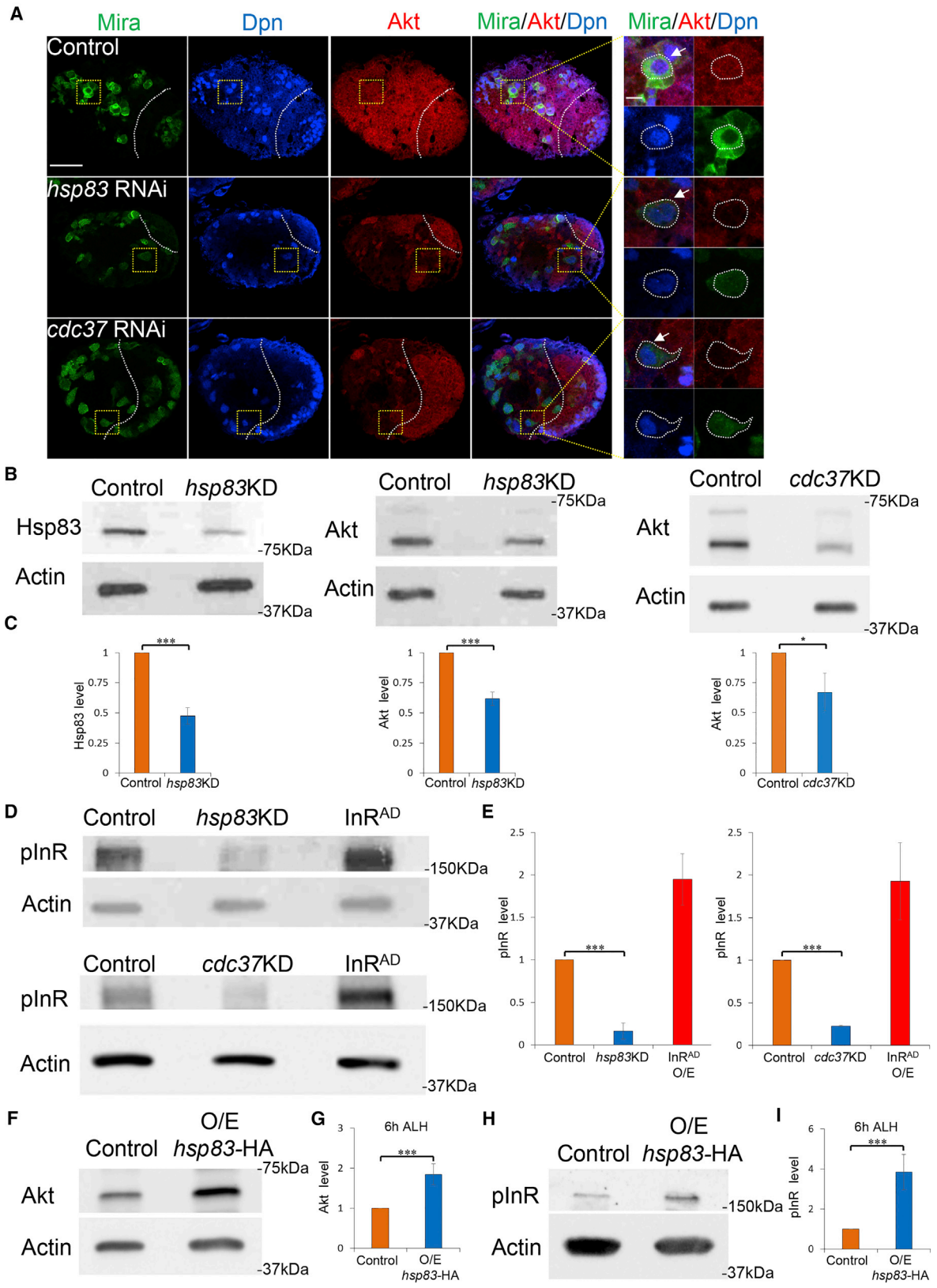
Taken together, we conclude that Hsp83 and Cdc37 are likely required for the activation of the InR/PI3K/Akt pathway.

Hsp83 Overexpression Results in Increase of pInR and Akt Level

Since Hsp83 overexpression triggers premature NSC reactivation, it is worthy to investigate whether Hsp83 overexpression can result in the activation of the InR/PI3K/Akt pathway. Due to insufficient amounts of protein that could be obtained due to the tiny size of larval brains at 6 hr ALH, we examined the protein levels of the whole larvae. Upon *hsp83*-HA overexpression in NSCs using *insc*-Gal4, the protein levels of Akt in the whole larvae were increased to 184.6% \pm 25.9% ($n = 4$), compared with controls (Figures 2F and 2G). Similarly, *hsp83* overexpression in NSCs resulted in a significant increase of pInR level in whole larvae, with 383.6% \pm 88.2% ($n = 4$) compared with controls (Figures 2H and 2I). These results suggest that overexpression of Hsp83 is sufficient to drive the activation of the InR/PI3K/Akt pathway on the fed condition.

Hsp83, Cdc37, and InR Physically Interact

Given that Hsp83 and Cdc37 are required for the activation of the InR/PI3K/Akt pathway, we explored whether Hsp83 and Cdc37 physically interact with InR or Akt. To test the physical association between Hsp83, Cdc37, and InR, we performed a proximity ligation assay (PLA), a technique



(legend on next page)



enabling high specificity and sensitivity detection of protein-protein interactions (Figure 3A) (Fredriksson et al., 2002). We co-expressed various proteins tagged with Myc or HA in S2 cells and quantified PLA foci that indicated interactions in cells, which co-expressed both Myc and HA-tagged proteins (Figures 3B and 3C). In S2 cells co-expressing both HA and Myc controls, the vast majority of cells (90.2%, $n = 1,397$) had no PLA signals and the rest of the cells displayed weak PLA fluorescence signal of less than 10 foci (Figures 3B and 3C). On average, these control cells only had 0.13 PLA foci per cell. We failed to generate full-length InR constructs, presumably due to its large size (>6 kb). As the intracellular domain of InR including the kinase domain (InR^{intra}), an active form of InR, was previously used for demonstrating protein-protein interactions for InR (Almudi et al., 2013), we decided to use InR^{intra} in PLA assays. Similarly, in the vast majority of cells co-expressing Myc-Hsp83 with control HA ($n = 1,456$) and HA-InR^{intra} with control Myc ($n = 1,767$), no PLA signal was detected and, on average, there were 0.45 and 0.38 PLA foci per cell, respectively (Figures 3B and 3C). By contrast, cells co-expressing Myc-Hsp83 and HA-InR^{intra} displayed 12.77 PLA foci per cell on average; 90.9% of cells exhibited PLA signal, with 41.8% of cells displaying moderate PLA signals (11–30 foci), 36.4% displaying weak PLA signals (≤ 10 foci), and 12.7% displaying strong PLA signals (>30 foci; Figures 3B and 3C; $n = 1784$). In a similar PLA assay, we tested whether Hsp83 interacts with Akt. The majority of S2 cells co-expressing Myc-Akt and HA-Hsp83 had no PLA signal (Figures S3A and S3B; 76.1%, $n = 1,581$), suggesting that Hsp83 did not interact with Akt. These results suggest that Hsp83 physically associated with InR^{intra}, but not Akt.

Similarly, in controls expressing Myc-Cdc37 and HA, we observed that the majority of cells (88.2%) had no PLA signal (Figures 3B and 3C; $n = 1,522$). However, co-expressing Myc-Cdc37 and HA-InR^{intra} resulted in 86.8% S2 cells showing PLA fluorescence; 51.3% of cells displayed weak PLA signals, 31.4% of cells showed moderate PLA signals, and 4.1% of

cells showed strong PLA signals (Figures 3B and 3C; $n = 1,144$). In controls co-expressing HA-Hsp83 and Myc, 88.5% of S2 cells did not have any PLA signal (Figures 3B and 3C; $n = 1,069$). By contrast, in cells co-expressing Myc-Cdc37 and HA-Hsp83, 51.5%, 30.4%, and 4.2% of these cells displayed weak, moderate, and strong PLA signals, respectively (Figures 3B and 3C; $n = 1,271$).

To further validate the interactions between Hsp83, Cdc37, and InR, we employed a protein-protein interaction assay named biomolecular fluorescence complementation (BiFC), which is able to detect transient or weak interactions due to the irreversibility of the BiFC complex formation (Gohl et al., 2010; Shyu and Hu, 2008). We generated chimeric proteins InR^{intra}-HA-CYFP (InR^{intra} with C-terminal YFP tagged with HA) and Hsp83-Myc-NYFP (N-terminal YFP tagged with Myc was fused to the Hsp83). As expected, when transfecting either of these two chimeric constructs into S2 cells with their respective controls, Myc-NYFP and HA-CYFP, no YFP signal was detected in cells (Figure S4B). By contrast, strong YFP was detected when cells were expressing both Hsp83-myc-NYFP and InR^{intra}-HA-CYFP, suggesting that Hsp83 and InR^{intra} physically associate (Figure S4B). To further test the specificity of this interaction, we generated a C-terminal truncation of Hsp83 (Figure S4A; Hsp83C: amino acids 538–717), which presumably abolishes the dimerization of Hsp83 and its subsequent ability to form a pocket-like structure to bind to its client proteins. We tested the ability of this Hsp83 truncation to associate with InR^{intra}. There was no YFP signal upon co-expression of Hsp83C-myc-NYFP with InR^{intra}-HA-CYFP in S2 cells (Figure S4B), suggesting that the association between Hsp83 and InR^{intra} was abolished with the N-terminal Hsp83 deletion. In addition, Hsp83 associated with its co-chaperone Cdc37, but not with an unrelated control WAVE in the BiFC assay (Figure S4B). Cdc37 also physically interacts with InR^{intra} in the BiFC assay, as S2 cells expressing both InR^{intra}-HA-CYFP and Cdc37-myc-NYFP, but not the controls, displayed YFP signal (Figure S4B).

Figure 2. Hsp83 and Cdc37 Are Required for the Activation of InR Pathway

(A) Larval brains of control (UAS-*dicer2*), *hsp83* RNAi (v108568), and *cdc37* RNAi (v47776) under *insc*-Gal4 at 72 hr ALH were stained for Mira, Dpn, and Akt. Yellow dotted boxes indicate the region of zoomed-in images. Central brain is to the left of white dotted lines. White arrows point to NSCs and outlines of NSCs are indicated by white dotted lines. Scale bars, 30 μ m for whole brain lobe and 5 μ m for single cell. (B and C) Western blot analysis of larval brain extracts of control (UAS-*dicer2*), *hsp83* knockdown (v108568), and *cdc37* knockdown (v110727) induced with *insc*-Gal4 at 72 hr ALH. Blots were probed with anti-Hsp83 antibody or anti-Akt antibody.

(D and E) Western blot analysis of larval brains of control (UAS-*dicer2*), *hsp83* knockdown (v108568), *cdc37* knockdown (v110727), and *InR*^{AD} overexpression (O/E; induced with *insc*-Gal4) at 72 hr ALH. Blots were probed with anti-pInR antibody.

(F and G) Western blot analysis of whole larvae extracts of control (UAS-*dicer2*), *hsp83*-HA overexpression induced with *insc*-Gal4 at 6 hr ALH. Blots were probed with anti-Akt antibody.

(H and I) Western blot analysis of whole larvae extracts of control (UAS-*dicer2*), *hsp83*-HA overexpression induced with *insc*-Gal4 at 6 hr ALH. Blots were probed with anti-pInR antibody. Loading control, actin (B, D, F, and H).

Statistical analyses were done comparing between two different genotypes using a two-tailed Student's t test (C, E, G, and I). * $p < 0.05$, *** $p < 0.001$. Data are presented as mean \pm SD in (C), (E), (G), and (I).

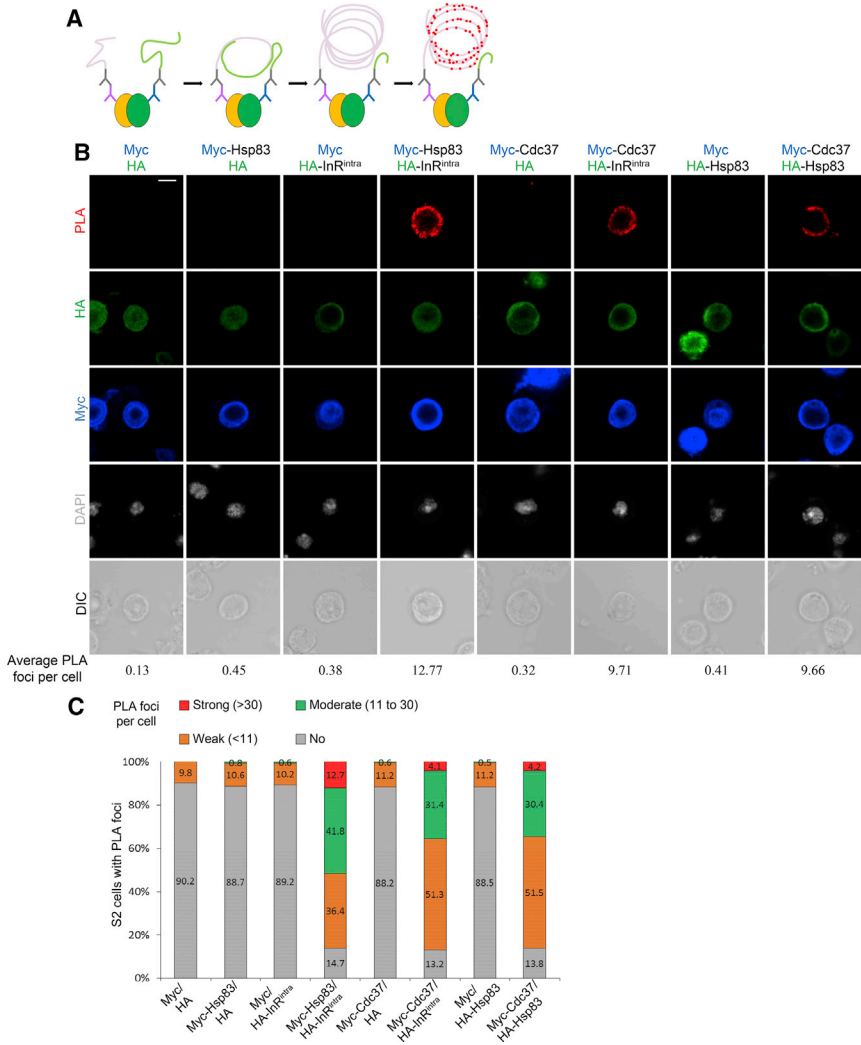


Figure 3. Hsp83, Cdc37, and InR Interact in PLA Assays

(A) A schematic representation of the proximity ligation assay performed on S2 cells (refer to [Experimental Procedures](#)).

(B) *In situ* PLA assay among Hsp83, Cdc37, and InR^{intra} in S2 cells. S2 cells transfected with two of the indicated plasmids (Myc, HA, Myc-Hsp83, HA-InR^{intra}, Myc-Cdc37, and HA-Hsp83) were stained for HA, Myc, and DNA and screened for PLA signal. Cell outline was determined by differential interference contrast images.

(C) Graphs showing the percentage of S2 cells with no PLA signal, and weak (≤ 10 foci), moderate (11–30 foci), and strong (>30 foci) PLA signals for (B). Scale bars, 4 μm .

Next, to examine their physical association in an *in vivo* BiFC assay, we generated transgenic flies expressing Hsp83-*myc*-NYFP, InR^{intra}-HA-CYFP, Cdc37-*myc*-NYFP, and Cdc37-HA-CYFP in NSCs under the *insc*-Gal4 driver. At 72 hr ALH at 29°C, overexpressed Hsp83, Cdc37, and InR^{intra} in NSCs were observed by their respective epitope tags. As expected, there was no detectable YFP when Hsp83-*myc*-NYFP, Cdc37-*myc*-NYFP, Cdc37-HA-CYFP Cdc37, or InR^{intra}-HA-CYFP were co-expressed with their corresponding control half-YFP proteins (Figure 4). By contrast, when Hsp83-*myc*-NYFP and InR^{intra}-HA-CYFP were co-expressed, strong YFP was detected in NSCs (Figure 4), suggesting that Hsp83 and InR^{intra} physically associate in NSCs. Likewise, Cdc37 interacted with both InR^{intra} and Hsp83 in NSCs in the BiFC assay (Figure 4). Taken together, Hsp83, Cdc37, and InR^{intra} physically associate with one another both *in vitro* and *in vivo* in BiFC assays.

Hsp83 Functions Upstream of the InR/PI3K/Akt Pathway in NSC Reactivation

Next, we ascertained whether Hsp83 functions upstream or downstream of the InR/PI3K/Akt pathway during NSC reactivation. Over-activation of the InR/PI3K/Akt pathway by expressing various active components of this pathway overrides the requirement of dietary amino acids for NSC reactivation (Chell and Brand, 2010; Sousa-Nunes et al., 2011). We explored whether depletion of *hsp83* was able to abrogate this effect of InR/PI3K/Akt pathway over-activation. Overexpression of an active form of InR (i.e., InR^{AD}, BDSC no. 8440) under the *insc*-Gal4 drove NSC reactivation in the absence of dietary amino acid (sucrose-only food), as there were 32.8 ± 13.9 ($n = 22$) EdU⁺ cells per brain hemisphere at 72 hr ALH (Figures 5A and 5B). Similarly, at the same growth condition, when *hsp83* was depleted in InR^{AD}-overexpressing brains, there were 32.5 ± 14.6 ($n = 25$) EdU⁺ cells per brain hemisphere (Figures 5A and 5B). Likewise, at 24 hr ALH in

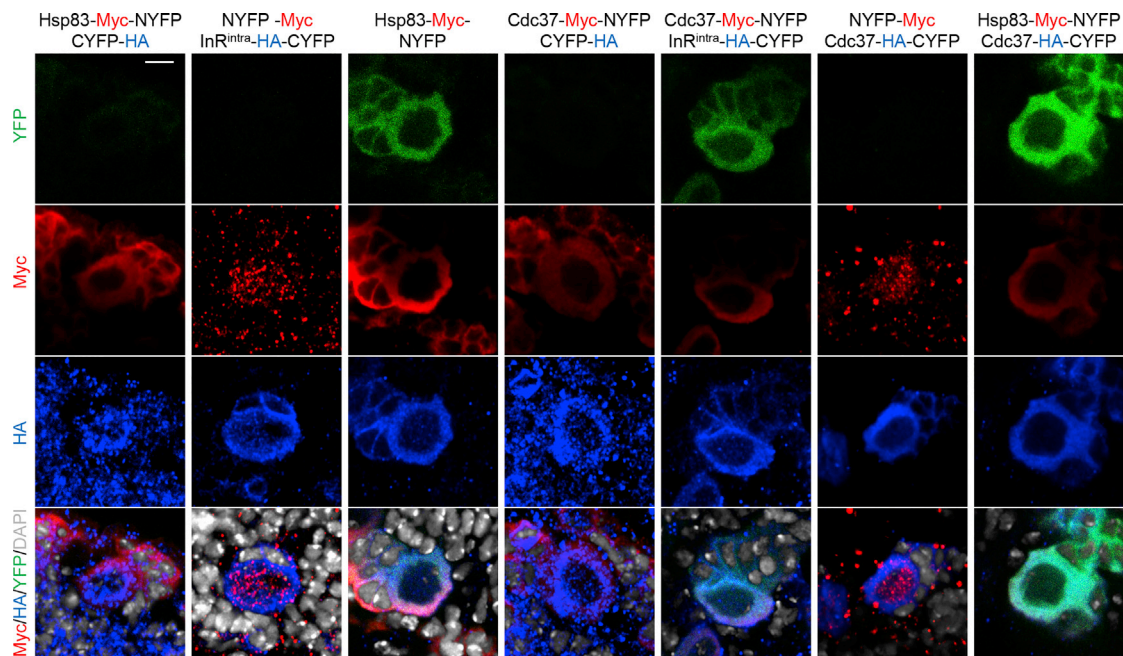


Figure 4. Hsp83, Cdc37, and InR Physically Associate in BiFC Assays

UAS-Hsp83-Myc-NYFP and UAS-InR^{intra}-HA-CYFP were co-expressed in larval NSCs by *insc*-Gal4 at 72 hr ALH, stained for Myc, HA, and DNA and screened for YFP fluorescence. Negative controls were UAS-Hsp83-Myc-NYFP with UAS-CYFP-HA and UAS-NYFP-Myc with UAS-InR^{intra}-HA-CYFP. Other transgenes used in the assay were UAS-Cdc37-Myc-NYFP and UAS-Cdc37-HA-CYFP. Scale bars, 4 μ m.

sucrose-only food, in InR^{AD}-overexpressing brains with *hsp83* RNAi knockdown, there were 17.1 ± 6.6 ($n = 20$) EdU⁺ cells per hemisphere (Figures S5A and S5B), similar to InR^{AD} overexpression alone (Figures S5A and S5B; 21.3 ± 5.0 EdU⁺ cells per hemisphere, $n = 32$). These observations suggest that over-activation of InR was epistatic to *hsp83* depletion in NSCs. Therefore, Hsp83 likely functions upstream of InR during NSC reactivation.

Rheb is a GTPase and a downstream effector of the InR/PI3K/Akt pathway in NSC reactivation (Shim et al., 2013). In sucrose-only food at 24 hr ALH, there were 15.2 ± 2.8 ($n = 42$) EdU⁺ cells per brain hemisphere upon Rheb^{wt} overexpression (wild-type form, BDSC no. 9689) under the *insc*-Gal4 (Figures S5B and S5D). Under the same conditions, 13.8 ± 3.4 EdU⁺ cells ($n = 48$) were observed in larval brains overexpressing Rheb^{wt} with *hsp83* RNAi knockdown (Figures S5B and S5D). Likewise, at 48 hr ALH on sucrose-only food, the number of EdU⁺ cells were similar in Rheb^{wt}-overexpressing brains with (Figures 5B and 5D; 21.6 ± 4.0 , $n = 26$) and without *hsp83* depletion (Figures 5B and 5D; 18.5 ± 4.2 , $n = 27$).

Under fed conditions, InR^{AD} or Rheb^{wt} overexpression also significantly rescued NSC quiescence phenotype caused by *hsp83* knockdown. At 48 hr ALH, vast majority of control NSCs were reactivated, except for $1.62\% \pm 0.8\%$ NSCs without EdU incorporation (Figures 5E and 5F; $n = 2410$, 24 brain lobes). Similarly, almost all NSCs

with InR^{AD} or Rheb^{wt} overexpression were reactivated as well, with none (Figures 5E and 5F; $n = 2,412$, 24 brain lobes) or $0.3\% \pm 0.4\%$ (Figures 5E and 5F; $n = 1,757$, 18 brain lobes) NSCs without EdU incorporation. Upon *hsp83* RNAi knockdown in NSCs, $48.9\% \pm 8.2\%$ (Figures 5E and 5F; $n = 1,357$, 17 brain lobes) lacked EdU incorporation. By contrast, at the same time point, in NSCs overexpressing InR^{AD} or Rheb^{wt} concomitant with *hsp83* RNAi knockdown, the percentages of EdU⁻ NSCs were decreased significantly to $11.7\% \pm 1.5\%$ (Figures 5E and 5F; $n = 2,392$, 26 brain lobes) and $10.4\% \pm 2.3\%$ (Figures 5E and 5F; $n = 1,827$, 22 brain lobes).

Taken together, overexpression of InR^{AD} or Rheb^{wt} significantly rescued NSC reactivation defects observed upon *hsp83* RNAi knockdown.

Amino Acids Deprivation Causes Significant Downregulation of *hsp83* mRNA and Inactivation of InR/PI3K/Akt Pathway

To explore whether the expression of *InR*, *hsp83*, and *cdc37* are nutrition dependent, we assessed the RNA level of *InR*, *hsp83*, and *cdc37* in larvae upon amino acid deprivation. At 24 hr ALH in sucrose-only food, the mRNA levels of *hsp83* were dramatically reduced to $13.4\% \pm 3.2\%$ and $10.4\% \pm 3.1\%$ measured by two different primer pairs ($n = 4$ each), compared with control larvae raised under fed conditions at the same time point (Figure S5E). RNA level of

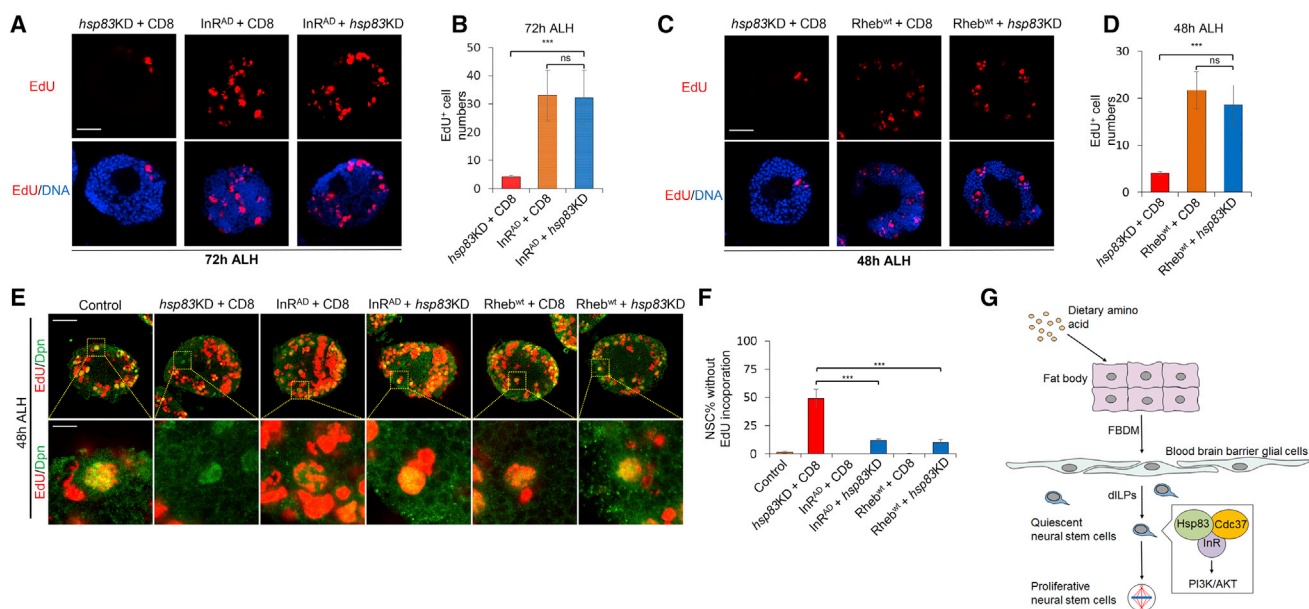


Figure 5. Hsp83 Functions Upstream of the InR/PI3K/Akt Pathway during NSC Reactivation

(A and B) Larval brains of *hsp83* knockdown (v108568) with UAS-CD8-GFP, *InR^{AD}* overexpression (BDSC no. 8440) with UAS-CD8-GFP, and *InR^{AD}* overexpression with *hsp83* knockdown (v108568) under *insc-Gal4* at 72 hr ALH in sucrose-only food were labeled with EdU and DNA. *hsp83* knockdown, 4.3 ± 0.5 (n = 16) EdU⁺ cells per brain hemisphere at 72 hr ALH.

(C and D) Larval brains of *hsp83* knockdown (v108568) with UAS-CD8-GFP, *Rheb^{wt}* overexpression (BDSC no. 9689) with UAS-CD8-GFP, and *Rheb^{wt}* overexpression with *hsp83* knockdown (v108568) under *insc-Gal4* at 48 hr ALH in sucrose-only food were labeled with EdU and DNA. *hsp83* knockdown, 4.0 ± 0.4 (n = 20) EdU⁺ cells per brain hemisphere at 48 hr ALH.

(E and F) Larval brains of control (UAS-*dicer2*), *hsp83* knockdown (v108568) with UAS-CD8-GFP, *InR^{AD}* overexpression (BDSC no. 8440) with UAS-CD8-GFP, *InR^{AD}* overexpression with *hsp83* knockdown (VDR no. 108568), *Rheb^{wt}* overexpression (BDSC no. 9689) with UAS-CD8-GFP, and *Rheb^{wt}* overexpression with *hsp83* knockdown (v108568) induced with *insc-Gal4* at 48 hr ALH in normal food were labeled with EdU and Dpn. Yellow dotted boxes indicate the region of zoomed-in images.

Data are presented in (B), (D), and (F) as mean ± SD. Statistical analyses were done by pairwise comparison between two different genotypes using a two-tailed Student's t test (B, D, and F). ns, not significant; ***p < 0.001. Scale bars, 15 μm in (A) and (C), 30 μm for whole brain lobe, and 5 μm for single cell in (E).

(G) A working model.

cdc37 remains unchanged on the starvation condition (Figure S5E). This suggests that the expression of *hsp83*, but not *cdc37*, is dependent on the presence of dietary amino acids. Surprisingly, the mRNA level of *InR* and *4E-binding protein* (*4E-BP*) on sucrose-only food was increased significantly to at least 5-fold (Figure S5E; n = 4). This result is in line with the previous finding that increased transcription of *InR* and *4E-BP* was correlated with inactivation of InR pathway and growth inhibition when nutrients are limited due to a feedback control mechanism for the InR pathway (Puig et al., 2003). Since the upregulation of mRNA levels of *InR* in the entire larvae upon amino acid deprivation was not observed in larval brains upon knocking down of *hsp83* alone, this effect likely involves additional factors that are altered by depletion of dietary amino acids or due to different experimental conditions. Therefore, amino acid deprivation causes dramatic downregulation of *hsp83* and inactivation of InR/PI3K/Akt pathway.

DISCUSSION

How the InR/PI3K/Akt pathway is regulated during NSC reactivation is poorly understood. Here we show that molecular chaperone Hsp83/Hsp90, together with its co-chaperone Cdc37, play a role in the reactivation of *Drosophila* NSCs. Mechanistically, Hsp83 and Cdc37 physically associate with InR and are important for the activation of the InR/PI3K/Akt pathway in NSCs. Therefore, we demonstrate that Hsp83 serves as an intrinsic factor within NSCs that is necessary for the activation of the InR/PI3K/Akt pathway and, in turn, reactivation of NSCs. Our evidence suggests that Hsp83 and Cdc37 regulate the protein folding and activation of InR in the nervous system.

The role of Hsp83 in NSC reactivation at early larval stages is distinct from its known role in centrosomes or NSC polarity. *Drosophila* Hsp83 is a core centrosomal component required for proper mitotic spindle formation



and chromosome segregation (Lange et al., 2000). In *Drosophila* larval CNS, Hsp83 and co-chaperone Sgt1 are required for the stabilization of Polo and centrosome organization in NSCs (Martins et al., 2009). Hsp83 and Sgt1 are also required for the establishment of NSC polarity via the LKB1/AMPK pathway in third-instar larvae (Andersen et al., 2012). However, *sgt1* RNAi (BDSC no. 34605) in NSCs did not display any phenotypes during NSC reactivation (data not shown), suggesting that Hsp83 interacts with different co-chaperones to control NSC reactivation and cortical polarity at different developmental stages. Consistent with this notion, we found that Cdc37, but not other co-chaperones of Hsp83, is required for NSC reactivation. We found that the proliferation of MB NSCs were unaffected by *hsp83* knockdown. Therefore, Hsp83 promotes NSC reactivation rather than general cell proliferation. Consistent with our observations, there is no significant difference in proliferation between *hsp83* mutant and wild-type eye imaginal discs in the proliferating zone (Bandura et al., 2013). Interestingly, in pupal eyes that undergo terminal differentiation, Hsp83 is required for cell-cycle exit by activating the anaphase-promoting complex/cyclosome (Bandura et al., 2013). We found cytokinesis defects in *cdc37*-depleted NSCs, but not in NSCs depleted of Hsp83 (data not shown). This observation is consistent with a known role of Cdc37 in cell division and cytokinesis in *Drosophila* (Lange et al., 2002).

Hsp90 plays a key role in signal transduction and appears to bind to its substrates in a near native state poised for activation by binding of ligand or other factors (Young et al., 2001). Since Hsp83 overexpression is sufficient to drive the activation of InR/PI3K/Akt pathway and trigger premature NSC reactivation, Hsp83 likely plays an active role in promoting NSC reactivation by binding to InR at a late stage of folding poised for activation by dILP binding. Furthermore, in the absence of dietary amino acids, the expression of *hsp83* is downregulated, likely partially contributing to the inactivation of the InR pathway (Figure S5E). We propose that InR is a target of Hsp83 and Cdc37 during NSC reactivation. The physical association among Hsp83, Cdc37, and InR was strongly supported by PLA assays, and both *in vitro* and *in vivo* BiFC. Although tandem affinity purification-mass spectrometry in *Drosophila* S2 cells implied an interaction between Hsp83 and InR (Friedman et al., 2011), we failed to detect a consistent interaction between Hsp83 and InR^{intra} in S2 cells in co-immunoprecipitation experiments, probably due to the transient nature of this interaction. In addition, our genetic interaction experiments indicate that Hsp83 activates the InR/PI3K/Akt pathway to promote NSC reactivation. Taken together, InR is likely a client of Hsp83 in *Drosophila* NSCs. Consistent with our findings, in human fibroblasts, Hsp90

co-immunoprecipitated with intracellular InR β subunit (Takata et al., 1997). Furthermore, Hsp90 facilitates the maturation of the InR precursor in the ER and, in turn, is required for cell surface expression of InR in both bovine adrenal medullary chromaffin cells and human kidney HEK293 cells (Ramos et al., 2007; Saitoh et al., 2002). Therefore, the interaction between the Hsp90 chaperone family and InR may be conserved from *Drosophila* to humans. In mammals, the expression level of Hsp90 in the brain is the highest among all tissues (Barrott and Haystead, 2013). Although mammalian Hsp90 proteins are heavily implicated in neurodegenerative diseases (Lackie et al., 2017; Luo et al., 2010), their function in brain development is not well understood. Hsp90/Cdc37 stabilize the intracellular domain of Ryk, a Wnt receptor required for neurogenesis (Lyu et al., 2009). Furthermore, Hsp90 stabilizes hypoxia-inducible factor-1, which promotes NSC proliferation under hypoxia (Xiong et al., 2009). It remains to be determined whether the interaction between mammalian Hsp90 and InR is conserved during mammalian NSC development.

EXPERIMENTAL PROCEDURES

Fly Stocks and Genetics

The fly strains used in this study were: UAS-CYFP-HA, UAS-NYFP-Myc, UAS-Hsp83-Myc-NYFP, UAS-InR^{intra}-HA-CYFP, UAS-Cdc37-Myc-NYFP, UAS-Cdc37-HA-CYFP, UAS-Hsp83-HA (T. Wang), *hsp83*-BAC, and *cdc37*-BAC. The following stocks were obtained from Bloomington *Drosophila* Stock Center (BDSC): RNAi for Hop and various isoforms of Hsp70 listed in Table S1, *cdc37* RNAi (BDSC no. 28756), *cdc37^{ex4D}* (BDSC no. 5693), UAS-InR.A1325D (InR^{AD}, BDSC no. 8440), UAS-Rheb^{wt} (BDSC no. 9689), and *hsp83^{ex6A}* (BDSC no. 36576). RNAi lines including *hsp83* RNAi (VDRC no. 108568) and *cdc37* RNAi (VDRC nos. 47776 and 110727) were obtained from Vienna *Drosophila* Resource Center (VDRC). *Hsp83^{5C2}* (DGRC no. 111379) was obtained from Kyoto *Drosophila* Genetic Resource Center. All experiments were carried out at 25°C, except for RNAi knockdown or overexpression at 29°C.

Immunocytochemistry

Larval brains were dissected in PBS and fixed for 22 min in 0.3% PBS-Triton (PBT) with 4% electron microscopy (EM)-grade formaldehyde (methanol free). Fixed brains were processed for immunostaining as described previously (Koe et al., 2014). Further details and primary antibodies used can be found in Supplemental Experimental Procedures.

MARCM Analysis

To generate MARCM clones, late first-instar larvae were heat shocked for 2 hr at 37°C, and heat shocked for a second time 10–16 hr later after recovering at 25°C. Larvae were dissected at the third instar-larval stage and for the tissue processed by immunocytochemistry.



EdU Pulse-Chase Analysis

Larvae were fed with standard food supplemented with 0.2 mM EdU from *Click-iT* EdU Alexa Fluor 555 Imaging Kit (Invitrogen) for 4 hr prior to dissection. The dissected larval brains were then fixed with 4% EM-grade formaldehyde (in 0.3% PBT) for 22 min. The brains were then processed for as described previously (Li et al., 2017).

SUPPLEMENTAL INFORMATION

Supplemental Information includes Supplemental Experimental Procedures, five figures, and three tables and can be found with this article online at <https://doi.org/10.1016/j.stemcr.2018.08.014>.

AUTHOR CONTRIBUTIONS

Conceptualization, H.W.; Methodology, H.J.; Writing – Original Draft, Review & Editing, H.W. and H.J.; Funding Acquisition, H.W.; Resources, H.W. and H.J.; Supervision, H.W.

ACKNOWLEDGMENTS

We thank H. Stocker, T. Wang, S. Bodgan, F. Matsuzaki, C. Doe, J. Knoblich, A.H. Brand, T. Lee, W. Chia, X. Yang, H. Steller, F. Yu, the Bloomington *Drosophila* Stock Center, Vienna *Drosophila* Resource Center, *Drosophila* Genomics Resource Center, and the Developmental Studies Hybridoma Bank for fly stocks and antibodies. We thank X. Wei for isolation of *hsp83* RNAi from the RNAi screen. This work is supported by Singapore National Medical Research Council (NMRC/CBRG/0082/2015).

Received: March 19, 2018

Revised: August 21, 2018

Accepted: August 21, 2018

Published: September 20, 2018

REFERENCES

- Ahn, S., and Joyner, A.L. (2005). In vivo analysis of quiescent adult neural stem cells responding to Sonic hedgehog. *Nature* 437, 894–897.
- Almudi, I., Poernbacher, I., Hafen, E., and Stocker, H. (2013). The Lnk/SH2B adaptor provides a fail-safe mechanism to establish the Insulin receptor-Chico interaction. *Cell Commun. Signal.* 11, 26.
- Andersen, R.O., Turnbull, D.W., Johnson, E.A., and Doe, C.Q. (2012). Sgt1 acts via an LKB1/AMPK pathway to establish cortical polarity in larval neuroblasts. *Dev. Biol.* 363, 258–265.
- Arsenijevic, Y., Weiss, S., Schneider, B., and Aebischer, P. (2001). Insulin-like growth factor-I is necessary for neural stem cell proliferation and demonstrates distinct actions of epidermal growth factor and fibroblast growth factor-2. *J. Neurosci.* 21, 7194–7202.
- Bandura, J.L., Jiang, H., Nickerson, D.W., and Edgar, B.A. (2013). The molecular chaperone Hsp90 is required for cell cycle exit in *Drosophila melanogaster*. *PLoS Genet.* 9, e1003835.
- Barrott, J.J., and Haystead, T.A. (2013). Hsp90, an unlikely ally in the war on cancer. *FEBS J.* 280, 1381–1396.
- Baser, A., Skabkin, M., and Martin-Villalba, A. (2017). Neural stem cell activation and the role of protein synthesis. *Brain Plast.* 3, 27–41.
- Britton, J.S., and Edgar, B.A. (1998). Environmental control of the cell cycle in *Drosophila*: nutrition activates mitotic and endoreplicative cells by distinct mechanisms. *Development* 125, 2149–2158.
- Chell, J.M., and Brand, A.H. (2010). Nutrition-responsive glia control exit of neural stem cells from quiescence. *Cell* 143, 1161–1173.
- Cloetta, D., Thomanetz, V., Baranek, C., Lustenberger, R.M., Lin, S., Oliveri, F., Atanasoski, S., and Ruegg, M.A. (2013). Inactivation of mTORC1 in the developing brain causes microcephaly and affects gliogenesis. *J. Neurosci.* 33, 7799–7810.
- Colombani, J., Raisin, S., Pantalacci, S., Radimerski, T., Montagne, J., and Leopold, P. (2003). A nutrient sensor mechanism controls *Drosophila* growth. *Cell* 114, 739–749.
- Cutforth, T., and Rubin, G.M. (1994). Mutations in Hsp83 and cdc37 impair signaling by the sevenless receptor tyrosine kinase in *Drosophila*. *Cell* 77, 1027–1036.
- Daynac, M., Chicheportiche, A., Pineda, J.R., Gauthier, L.R., Bousin, F.D., and Mouthon, M.A. (2013). Quiescent neural stem cells exit dormancy upon alteration of GABAAR signaling following radiation damage. *Stem Cell Res.* 11, 516–528.
- Daynac, M., Tirou, L., Faure, H., Mouthon, M.A., Gauthier, L.R., Hahn, H., Bousin, F.D., and Ruat, M. (2016). Hedgehog controls quiescence and activation of neural stem cells in the adult ventricular-subventricular zone. *Stem Cell Rep.* 7, 735–748.
- Ding, R., Weynans, K., Bossing, T., Barros, C.S., and Berger, C. (2016). The Hippo signalling pathway maintains quiescence in *Drosophila* neural stem cells. *Nat. Commun.* 7, 10510.
- Doetsch, F., Garcia-Verdugo, J.M., and Alvarez-Buylla, A. (1999). Regeneration of a germinal layer in the adult mammalian brain. *Proc. Natl. Acad. Sci. USA* 96, 11619–11624.
- Eckl, J.M., and Richter, K. (2013). Functions of the Hsp90 chaperone system: lifting client proteins to new heights. *Int. J. Biochem. Mol. Biol.* 4, 157–165.
- Faiz, M., Sachewsky, N., Gascon, S., Bang, K.W., Morshead, C.M., and Nagy, A. (2015). Adult neural stem cells from the subventricular zone give rise to reactive astrocytes in the cortex after stroke. *Cell Stem Cell* 17, 624–634.
- Fredriksson, S., Gullberg, M., Jarvius, J., Olsson, C., Pietras, K., Gustafsdottir, S.M., Ostman, A., and Landegren, U. (2002). Protein detection using proximity-dependent DNA ligation assays. *Nat. Biotechnol.* 20, 473–477.
- Friedman, A.A., Tucker, G., Singh, R., Yan, D., Vinayagam, A., Hu, Y., Binari, R., Hong, P., Sun, X., Porto, M., et al. (2011). Proteomic and functional genomic landscape of receptor tyrosine kinase and ras to extracellular signal-regulated kinase signaling. *Sci. Signal.* 4, rs10.
- Göhl, C., Banovic, D., Grevelhorster, A., and Bogdan, S. (2010). WAVE forms hetero- and homo-oligomeric complexes at integrin junctions in *Drosophila* visualized by bimolecular fluorescence complementation. *J. Biol. Chem.* 285, 40171–40179.
- Isshiki, T., Pearson, B., Holbrook, S., and Doe, C.Q. (2001). *Drosophila* neuroblasts sequentially express transcription factors



which specify the temporal identity of their neuronal progeny. *Cell* 106, 511–521.

Ito, K., and Hotta, Y. (1992). Proliferation pattern of postembryonic neuroblasts in the brain of *Drosophila melanogaster*. *Dev. Biol.* 149, 134–148.

Juanes, M., Guercio, G., Marino, R., Berensztein, E., Warman, D.M., Ciaccio, M., Gil, S., Bailez, M., Rivarola, M.A., and Belgorosky, A. (2015). Three novel IGF1R mutations in microcephalic patients with prenatal and postnatal growth impairment. *Clin. Endocrinol. (Oxf)* 82, 704–711.

Kawai, H., Kawaguchi, D., Kuebrich, B.D., Kitamoto, T., Yamaguchi, M., Gotoh, Y., and Furutachi, S. (2017). Area-specific regulation of quiescent neural stem cells by Notch3 in the adult mouse subependymal zone. *J. Neurosci.* 37, 11867–11880.

Koe, C.T., Li, S., Rossi, F., Wong, J.J., Wang, Y., Zhang, Z., Chen, K., Aw, S.S., Richardson, H.E., Robson, P., et al. (2014). The Brm-HDAC3-Erm repressor complex suppresses dedifferentiation in *Drosophila* type II neuroblast lineages. *Elife* 3, e01906.

Kuo, Y., Ren, S., Lao, U., Edgar, B.A., and Wang, T. (2013). Suppression of polyglutamine protein toxicity by co-expression of a heat-shock protein 40 and a heat-shock protein 110. *Cell Death Dis.* 4, e833.

Lackie, R.E., Maciejewski, A., Ostapchenko, V.G., Marques-Lopes, J., Choy, W.Y., Duennwald, M.L., Prado, V.F., and Prado, M.A.M. (2017). The Hsp70/Hsp90 chaperone machinery in neurodegenerative diseases. *Front. Neurosci.* 11, 254.

Lai, S.L., and Doe, C.Q. (2014). Transient nuclear Prospero induces neural progenitor quiescence. *Elife* 3. <https://doi.org/10.7554/eLife.03363>.

Lange, B.M., Bachi, A., Wilm, M., and Gonzalez, C. (2000). Hsp90 is a core centrosomal component and is required at different stages of the centrosome cycle in *Drosophila* and vertebrates. *EMBO J.* 19, 1252–1262.

Lange, B.M., Rebollo, E., Herold, A., and Gonzalez, C. (2002). Cdc37 is essential for chromosome segregation and cytokinesis in higher eukaryotes. *EMBO J.* 21, 5364–5374.

Lee, T., and Luo, L. (2001). Mosaic analysis with a repressible cell marker (MARCM) for *Drosophila* neural development. *Trends Neurosci.* 24, 251–254.

Li, S., Koe, C.T., Tay, S.T., Tan, A.L.K., Zhang, S., Zhang, Y., Tan, P., Sung, W.K., and Wang, H. (2017). An intrinsic mechanism controls reactivation of neural stem cells by spindle matrix proteins. *Nat. Commun.* 8, 122.

Lugert, S., Basak, O., Knuckles, P., Haussler, U., Fabel, K., Gotz, M., Haas, C.A., Kempermann, G., Taylor, V., and Giachino, C. (2010). Quiescent and active hippocampal neural stem cells with distinct morphologies respond selectively to physiological and pathological stimuli and aging. *Cell Stem Cell* 6, 445–456.

Luo, W., Sun, W., Taldone, T., Rodina, A., and Chiosis, G. (2010). Heat shock protein 90 in neurodegenerative diseases. *Mol. Neurodegener.* 5, 24.

Lyu, J., Wesselschmidt, R.L., and Lu, W. (2009). Cdc37 regulates Ryk signaling by stabilizing the cleaved Ryk intracellular domain. *J. Biol. Chem.* 284, 12940–12948.

Mairet-Coello, G., Tury, A., and DiCicco-Bloom, E. (2009). Insulin-like growth factor-1 promotes G(1)/S cell cycle progression through bidirectional regulation of cyclins and cyclin-dependent kinase inhibitors via the phosphatidylinositol 3-kinase/Akt pathway in developing rat cerebral cortex. *J. Neurosci.* 29, 775–788.

Martins, T., Maia, A.F., Steffensen, S., and Sunkel, C.E. (2009). Sgt1, a co-chaperone of Hsp90 stabilizes Polo and is required for centrosome organization. *EMBO J.* 28, 234–247.

Morshead, C.M., Reynolds, B.A., Craig, C.G., McBurney, M.W., Staines, W.A., Morassutti, D., Weiss, S., and van der Kooy, D. (1994). Neural stem cells in the adult mammalian forebrain: a relatively quiescent subpopulation of subependymal cells. *Neuron* 13, 1071–1082.

Poon, C.L., Mitchell, K.A., Kondo, S., Cheng, L.Y., and Harvey, K.F. (2016). The hippo pathway regulates neuroblasts and brain size in *Drosophila melanogaster*. *Curr. Biol.* 26, 1034–1042.

Pratt, W.B., and Toft, D.O. (1997). Steroid receptor interactions with heat shock protein and immunophilin chaperones. *Endocr. Rev.* 18, 306–360.

Puig, O., Marr, M.T., Ruhf, M.L., and Tjian, R. (2003). Control of cell number by *Drosophila* FOXO: downstream and feedback regulation of the insulin receptor pathway. *Genes Dev.* 17, 2006–2020.

Ramos, R.R., Swanson, A.J., and Bass, J. (2007). Calreticulin and Hsp90 stabilize the human insulin receptor and promote its mobility in the endoplasmic reticulum. *Proc. Natl. Acad. Sci. USA* 104, 10470–10475.

Saitoh, T., Yanagita, T., Shiraishi, S., Yokoo, H., Kobayashi, H., Minami, S., Onitsuka, T., and Wada, A. (2002). Down-regulation of cell surface insulin receptor and insulin receptor substrate-1 phosphorylation by inhibitor of 90-kDa heat-shock protein family: endoplasmic reticulum retention of monomeric insulin receptor precursor with calnexin in adrenal chromaffin cells. *Mol. Pharmacol.* 62, 847–855.

Sawarkar, R., Sievers, C., and Paro, R. (2012). Hsp90 globally targets paused RNA polymerase to regulate gene expression in response to environmental stimuli. *Cell* 149, 807–818.

Shim, J., Gururaja-Rao, S., and Banerjee, U. (2013). Nutritional regulation of stem and progenitor cells in *Drosophila*. *Development* 140, 4647–4656.

Shyu, Y.J., and Hu, C.D. (2008). Fluorescence complementation: an emerging tool for biological research. *Trends Biotechnol.* 26, 622–630.

Sousa-Nunes, R., Yee, L.L., and Gould, A.P. (2011). Fat cells reactivate quiescent neuroblasts via TOR and glial insulin relays in *Drosophila*. *Nature* 471, 508–512.

Speder, P., and Brand, A.H. (2014). Gap junction proteins in the blood-brain barrier control nutrient-dependent reactivation of *Drosophila* neural stem cells. *Dev. Cell* 30, 309–321.

Speder, P., and Brand, A.H. (2018). Systemic and local cues drive neural stem cell niche remodelling during neurogenesis in *Drosophila*. *Elife* 7.

Takata, Y., Imamura, T., Iwata, M., Usui, I., Haruta, T., Nandachi, N., Ishiki, M., Sasaoka, T., and Kobayashi, M. (1997). Functional importance of heat shock protein 90 associated with insulin



- receptor on insulin-stimulated mitogenesis. *Biochem. Biophys. Res. Commun.* *237*, 345–347.
- Tariq, M., Nussbaumer, U., Chen, Y., Beisel, C., and Paro, R. (2009). Trithorax requires Hsp90 for maintenance of active chromatin at sites of gene expression. *Proc. Natl. Acad. Sci. USA* *106*, 1157–1162.
- Truman, J.W., and Bate, M. (1988). Spatial and temporal patterns of neurogenesis in the central nervous system of *Drosophila melanogaster*. *Dev. Biol.* *125*, 145–157.
- Tsuji, T., Hasegawa, E., and Isshiki, T. (2008). Neuroblast entry into quiescence is regulated intrinsically by the combined action of spatial Hox proteins and temporal identity factors. *Development* *135*, 3859–3869.
- Wang, Y.Z., Plane, J.M., Jiang, P., Zhou, C.J., and Deng, W. (2011). Concise review: quiescent and active states of endogenous adult neural stem cells: identification and characterization. *Stem Cells* *29*, 907–912.
- Xiong, L., Zhao, T., Huang, X., Liu, Z.H., Zhao, H., Li, M.M., Wu, L.Y., Shu, H.B., Zhu, L.L., and Fan, M. (2009). Heat shock protein 90 is involved in regulation of hypoxia-driven proliferation of embryonic neural stem/progenitor cells. *Cell Stress Chaperones* *14*, 183–192.
- Yan, Y.P., Sailor, K.A., Vemuganti, R., and Dempsey, R.J. (2006). Insulin-like growth factor-1 is an endogenous mediator of focal ischemia-induced neural progenitor proliferation. *Eur. J. Neurosci.* *24*, 45–54.
- Ye, P., Popken, G.J., Kemper, A., McCarthy, K., Popko, B., and D’Ercole, A.J. (2004). Astrocyte-specific overexpression of insulin-like growth factor-I promotes brain overgrowth and glial fibrillary acidic protein expression. *J. Neurosci. Res.* *78*, 472–484.
- Young, J.C., Moarefi, I., and Hartl, F.U. (2001). Hsp90: a specialized but essential protein-folding tool. *J. Cell Biol.* *154*, 267–273.

Stem Cell Reports, Volume 11

Supplemental Information

**Hsp83/Hsp90 Physically Associates with Insulin Receptor to Promote
Neural Stem Cell Reactivation**

Jiawen Huang and Hongyan Wang

SUPPLEMENTAL TABLES**Table S1. Knockdown of hsp70 did not result in defects in NSC reactivation**

S/N	Isoforms of Hsp70	RNAi stock number	NSC reactivation defects
1	Hsp70Aa	BDSC#42639	No
2	Hsp70Ab	BDSC#35663	No
3	Hsp70Ba	BDSC#35672	No
4		BDSC#43289	No
5	Hsp70Bb	BDSC#32997	No
6		BDSC#33948	No
7	Hsp70Bbb	BDSC#28787	No
8		BDSC#33000	No
9		BDSC#33916	No
10	Hsp70Bc	BDSC#35697	No
11		BDSC#42626	No
12	Hsc70-4	BDSC#28709	No
13		BDSC#35684	No
14		BDSC#54810	No
15	Hop	BDSC#32979	No
16		BDSC#34002	No

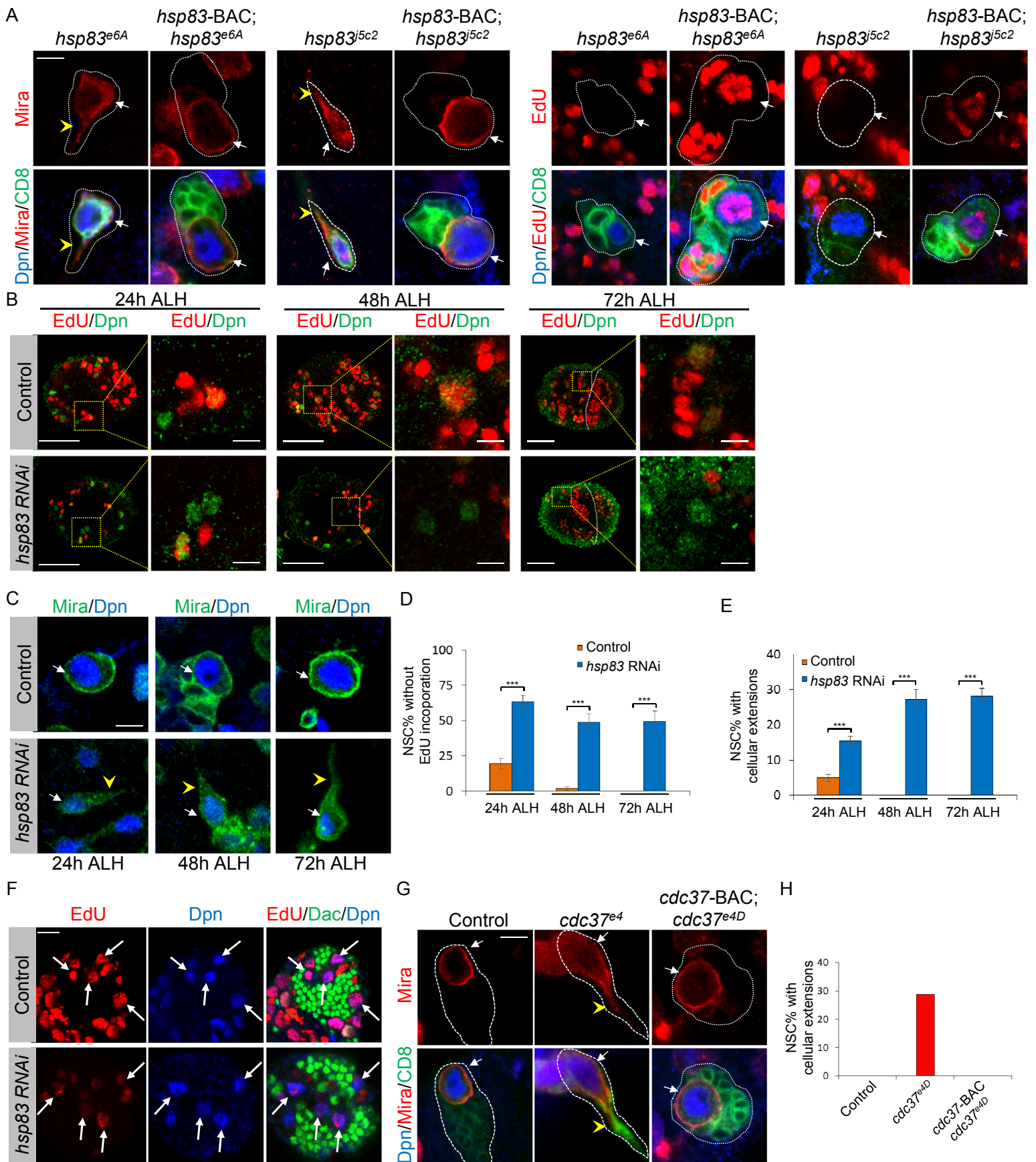
Table S2: Lists of primers used to generate generate entry clones for Hsp83, InR^{intra} and Cdc37 and proper controls

Primer name	Primer Sequence (5'-3')	Purpose
BP.Hsp83.F	GGGG ACA AGT TTG TAC AAA AAA GCA GGC TTC ATG CCA GAA GAA GCA GAG ACC	To generate pDONR211-Hsp83
BP.Hsp83.stop.R	GGGG AC CAC TTT GTA CAA GAA AGC TGG GTC TTA ATC GAC CTC CTC CAT GTG GGA A	
BP.Hsp83.no-stop.R	GGGG AC CAC TTT GTA CAA GAA AGC TGG GTC ATC GAC CTC CTC CAT GTG GGA AGC G	To generate pDONR211-Hsp83 without stop codon
BP.Hsp83C.F	GGGG ACA AGT TTG TAC AAA AAA GCA GGC TTC GAG GAT GAG AGC GAG AAG AAG	To generate pDONR211-Hsp83C without stop codon
BP.InRintra.F	GGGG ACA AGT TTG TAC AAA AAA GCA GGC TTC ATG ATT CAG TTG GCT CCA CTA	To generate pDONR211-InR ^{intra}
BP.InRintra.stop.R	GGGG AC CAC TTT GTA CAA GAA AGC TGG GTC TTA CGC CTC CCT TCC GAT G	
BP.InRintra.no-stop.R	GGGG AC CAC TTT GTA CAA GAA AGC TGG GTC TTT CGC CTC CCT TCC GAT G	To generate pDONR211-InR ^{intra} without stop codon
BP.Cdc37.F	GGGG ACA AGT TTG TAC AAA AAA GCA GGC TTC ATG GTG GAC TAC AGC AAG TGG	To generate pDONR211-Cdc37
BP.Cdc37.stop.R	GGGG AC CAC TTT GTA CAA GAA AGC TGG GTC TCA GTC AAC GTC CTC GGT GCT GAC G	
BP.Cdc37.no-stop.R	GGGG AC CAC TTT GTA CAA GAA AGC TGG GTC GTC AAC GTC CTC GGT GCT GAC GCC A	To generate pDONR211-Cdc37 without stop codon
BP.2HA.F	GGGG ACA AGT TTG TAC AAA AAA GCA GGC TTC ATG TAC CCA TAC GAT GTT CCA GAT TAC GCT GGA TAT CCG T	To generate pDONR211-2xHA without stop codon
BP.2HA.no-stop.R	GGGG AC CAC TTT GTA CAA GAA AGC TGG GTC TGC ATA GTC AGG CAC GTC ATA CGG ATA TCC AGC GTA ATC T	
BP.3Myc.F	GGGG ACA AGT TTG TAC AAA AAA GCA GGC TTC ATG GAA CAA AAA CTC ATC TCA GAA GAG GAT CTG GGA GAG CAG AAG CTA ATA TCT GAG GAA G	To generate pDONR211-3xMyc without stop codon
BP.3Myc.no-stop.R	GGGG AC CAC TTT GTA CAA GAA AGC TGG GTC TAG ATC TTC TTC CGA AAT AAG TTT CTG TTC TCC GAG GTC TTC CTC AGA TAT TAG CTT C	
Modifier pD221 F	GGGG ACAAGTTTGTACAAAAAAGCAGGCTTC GGTACCGCTGAAACGAAGTTAACTTTGAGGT GTACGGGTAAGTATTAGAAAGCAGGACTAAAC G	To generate pDONR211-Modifier to remove RfB cassette from BiFC, PAHW and PAMW constructs
Modifier pD221 R	GGGG ACCACTTTGTACAAGAAAGCTGGGTC AAGCTTCTATTCAATGGTCCGGCGGCCGACGAC ATGAGGATATGGTCGTTTAGTCCTGCTTTCTAA	

F: forward primer; R: reverse primer

Table S3: List of primers used for qPCR

Genes	Primer sequence (5' to 3')	
Hsp83-1	Forward	TCTACAAATCCCTGACCAAC
	Reverse	GTTCTTGCTGAACTGGTCAT
Hsp83-2	Forward	GGTGTGCGTCGTAACAACAAGC
	Reverse	CATCAGCTGAGCAATCTCAGCCT
Cdc37	Forward	CACTCACCCAAACATAGACA
	Reverse	TTTTCGAGCTCTTTCTTCAG
InR-1	Forward	GAATGGATCGTCTGACAAAT
	Reverse	GCGACTTCTTAAACTGGTG
InR-2	Forward	CTCAGCCATAACCAGGGACTTT
	Reverse	CTCTCCATAACACCGCCATC
InR-3	Forward	GTCACAATATTTTGCGAACA
	Reverse	TTGGCCAGTAGGATAAAGAG
Akt	Forward	ACCTACCGTTTGTCTTCAG
	Reverse	TAACCCATCAGTCTTCCATC
4E-BP	Forward	CTCCTGGAGGCACCAAACCTTATC
	Reverse	TTCCCCTCAGCAAGCAACTG
Actin5C	Forward	CAGATCATGTTTCGAGACCTTCA
	Reverse	TCATGATGGAGTTGTAGGTGGT
GADPH1	Forward	ATGACGAAATCAAGGCTAAG
	Reverse	GAGTAACCGAACTCGTTGTC
GADPH2	Forward	ATGAAATTAAGGCCAAGGTT
	Reverse	GAGTAGCCAAACTCGTTGTC
G6DPH	Forward	ACGAGCAGAAGAAGTACGAG
	Reverse	GATGTTGACAGTCACCTCCT
RPII215	Forward	ACGAGCGATTAATGAAAAAG
	Reverse	TCTGCACATTCCAGATCATA



SUPPLEMENTAL FIGURE LEGNEDS

Figure S1. Hsp83 and its co-chaperone Cdc37 contribute to NSC reactivation

(A) Larval NSC clones of *hsp83^{ε6A}*, *hsp83^{ε6A}* with *hsp83*-BAC, *hsp83^{5C2}*, *hsp83^{5C2}* with *hsp83*-BAC, at 96h ALH were stained for GFP (green), Dpn (blue) and Mira (red) or labeled with GFP (green), Dpn (blue) and EdU (red). NSC lineages were marked with CD8-GFP. White arrows point to NSCs and yellow arrowheads point to cellular extensions of NSCs. Clone outline is indicated by white dotted lines. Scale bars, 5 μm. (B) Larval brains of control (UAS-*dicer2*) and *hsp83* RNAi (VDRC#108568) under the control of *insc*-Gal4 at 24h, 48h and 72h ALH were labeled with EdU (red) and Dpn (green). Yellow dotted boxes indicate the region of zoomed-in images. Central brain is to the left of white dotted lines. Scale bars, 30 μm for whole brain lobe and 5 μm for single cell. (C) Larval brains of control (UAS-*dicer2*) and *hsp83* RNAi (VDRC#108568) induced with *insc*-Gal4 at 24h, 48h and 72h ALH were stained for Mira (green) and Dpn (blue). White arrows point to NSCs and yellow arrowheads point to cellular extensions of NSC. Scale bars, 5 μm. (D, E) Quantification of EdU incorporation (D) and cellular extensions (E) for control and *hsp83* RNAi in (C). Data are presented as mean ± SD. (F) Larval brains of control (UAS-*dicer2*) and *hsp83* RNAi (VDRC#108568) induced with *insc*-Gal4 at 24h ALH were stained for Dac (green), EdU (red) and Dpn (blue). Arrows point to MB NSCs. Scale bars, 10 μm. (G) Larval NSC clones of wild-type control, *cdc37^{ε4D}*, and *cdc37^{ε4D}* with *cdc37*-BAC at 96h ALH were stained for GFP (green), Dpn (blue) and Mira (red). NSC lineages were marked with CD8-GFP. White arrows point to NSCs and yellow arrowheads point to cellular extensions of NSC. Clone outline is indicated by white dotted lines. Scale bars, 5 μm. (H) Quantification of cellular extensions for control, *cdc37^{ε4D}*, and *cdc37^{ε4D}* with *cdc37*-BAC in (G). Data are presented as mean ± SD (D, E). Statistical analyses were done comparing between two different genotypes using two-tailed Student's *t*-test (D, E). ****P* < 0.001.

Figure S2

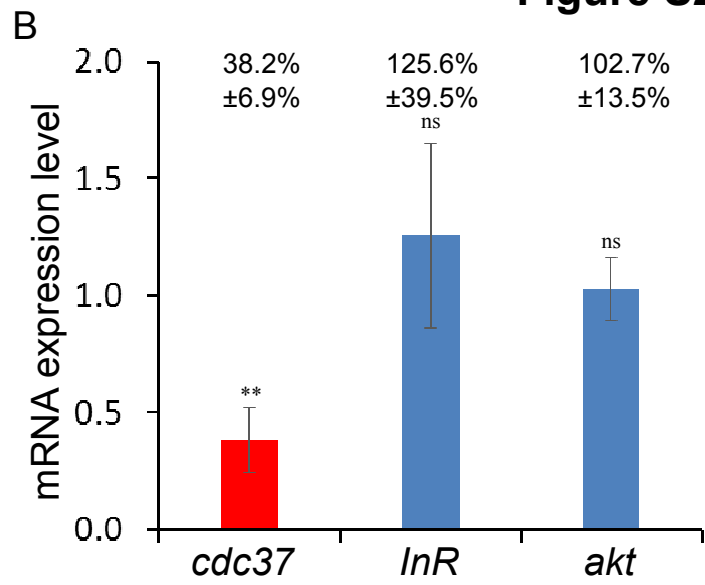
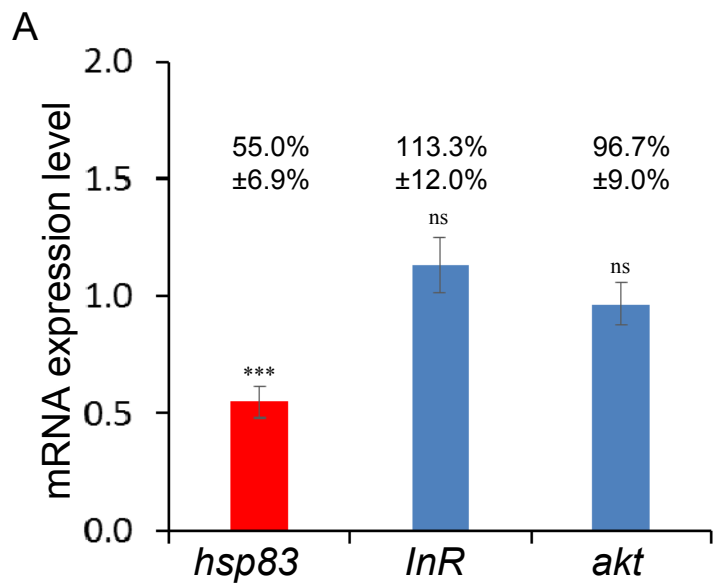
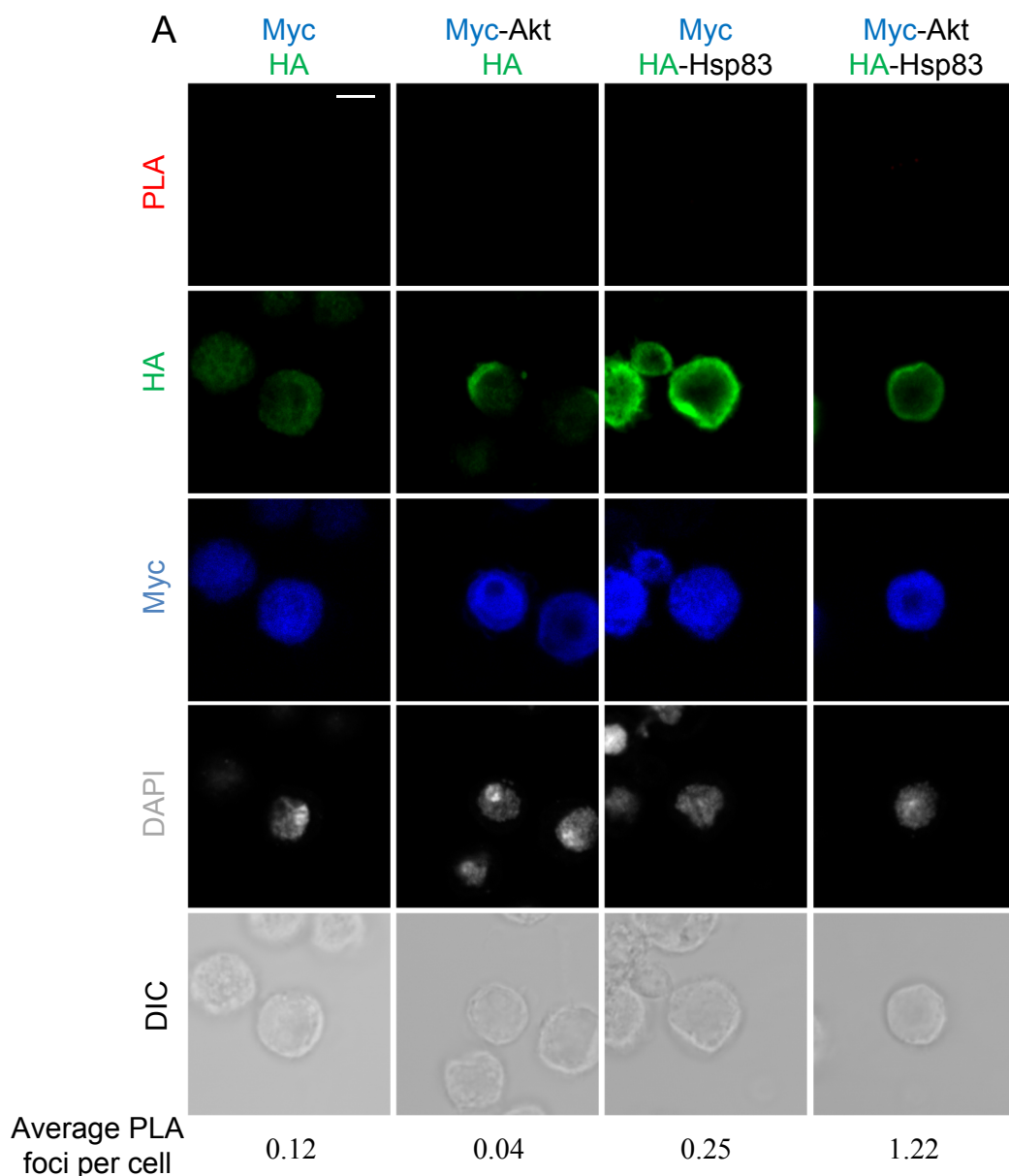


Figure S2. mRNA levels of InR and akt remain unaltered upon *hsp83* and *cdc37* knockdown in larval brains

(A) qPCR analysis of *hsp83*, *InR* and *akt* in larval brains of control (UAS-*dicer2*) and *hsp83* RNAi (VDRC#108568) under *insc*-Gal4 at 72h ALH. n=3. Statistical analyses were done comparing between control (actin5C and GADPH1) and *hsp83* knockdown, using two-tailed Student's *t*-test. The mRNA levels of control were normalized to 1. ns: non-significant; *** $P < 0.001$. (B) qPCR analysis of *cdc37*, *InR* and *akt* in larval brains of control (UAS-*dicer2*) and *cdc37* RNAi (VDRC#110727; induced with *insc*-Gal4) at 72h ALH. n=3. The mRNA levels of internal control (actin5C and GADPH1) was normalized to 1. Statistical analyses were done comparing between control and *cdc37* knockdown using two-tailed Student's *t*-test. ns: non-significant; ** $P < 0.01$.

Figure S3



B PLA foci per cell

- Strong (>30)
- Moderate (11 to 30)
- Weak (<11)
- No

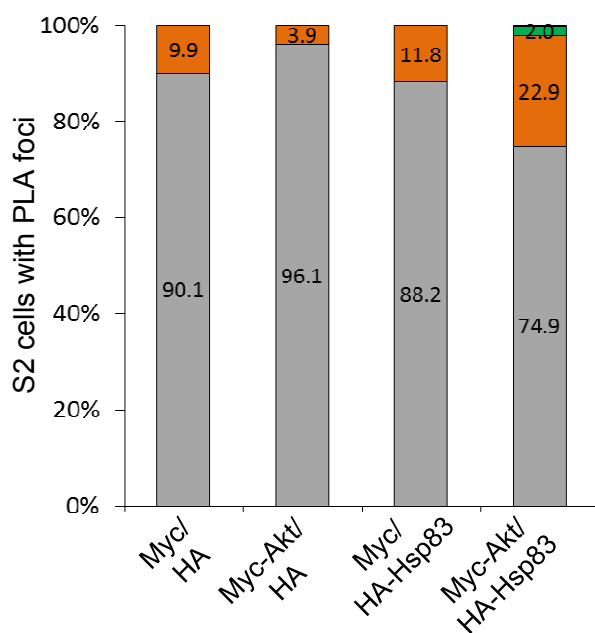


Figure S3. Hsp83 does not interact with Akt

(A) *In situ* PLA assay between Hsp83 and Akt in S2 cells. S2 cells transfected with two of the indicated plasmids (Myc, HA, Myc-Akt and HA-Hsp83) were stained for HA (green), Myc (blue) and DNA (grey) and detected for PLA signal (red). Cell outline was shown by differential interference contrast (DIC) images. Scale bars, 4 μ m. (B) Graphs showing the percentage of S2 cells with no PLA signal (grey), weak (≤ 10 foci, orange), moderate (11-30 foci, green) and strong (>30 foci, red) PLA signals for (A).

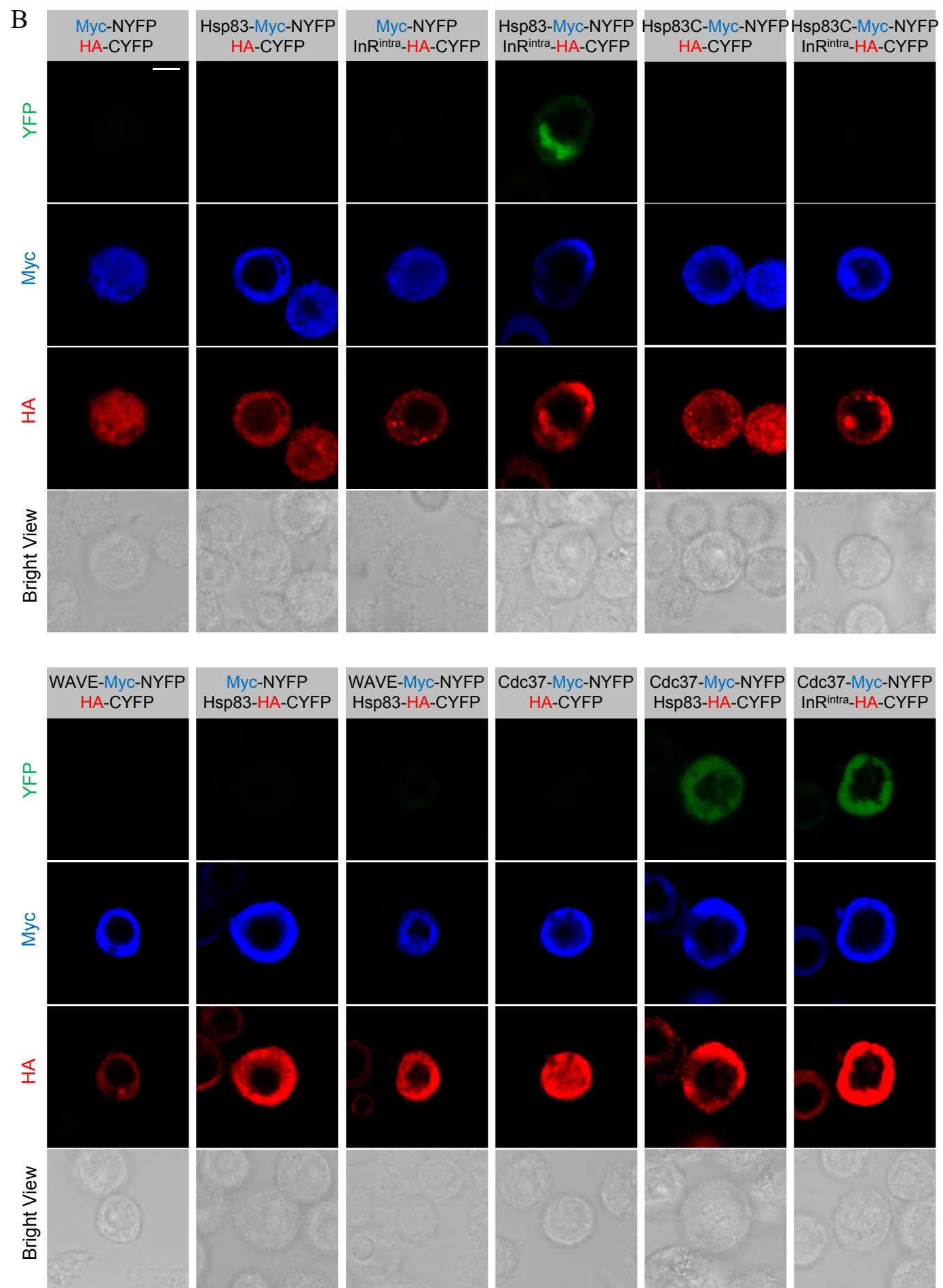
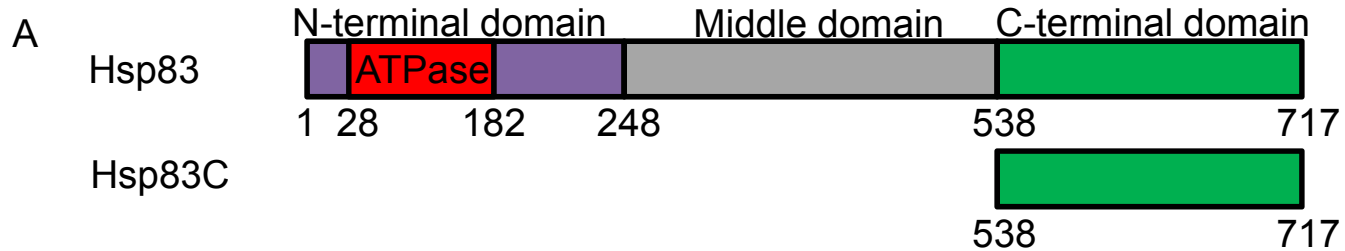


Figure S4. BiFC assays for Hsp83, Cdc37 and InR^{intra} interaction in S2 cells

(A) A schematic representation of the Hsp83C fragment. Hsp83C contains only the C-terminal domain of Hsp83 (538-717 amino acids). (B) Hsp83, Cdc37 and InR^{intra} interact in BiFC assays. To test the interaction between Hsp83 and InR^{intra}, UAS-Hsp83-Myc-NYFP and UAS-InR^{intra}-HA-CYFP were co-transfected into S2 cells, stained for Myc (blue) and HA (red) and detected for YFP fluorescence (green). Plasmids used for negative controls were UAS-Hsp83C-Myc-NYFP, UAS-HA-CYFP, UAS-Myc-NYFP and UAS-WAVE-Myc-NYFP. UAS-Cdc37-Myc-NYFP and UAS-Hsp83-HA-CYFP were used to test interaction between Cdc37 and Hsp83. Expression was induced by *actin*-Gal4. Scale bars, 4 μ m.

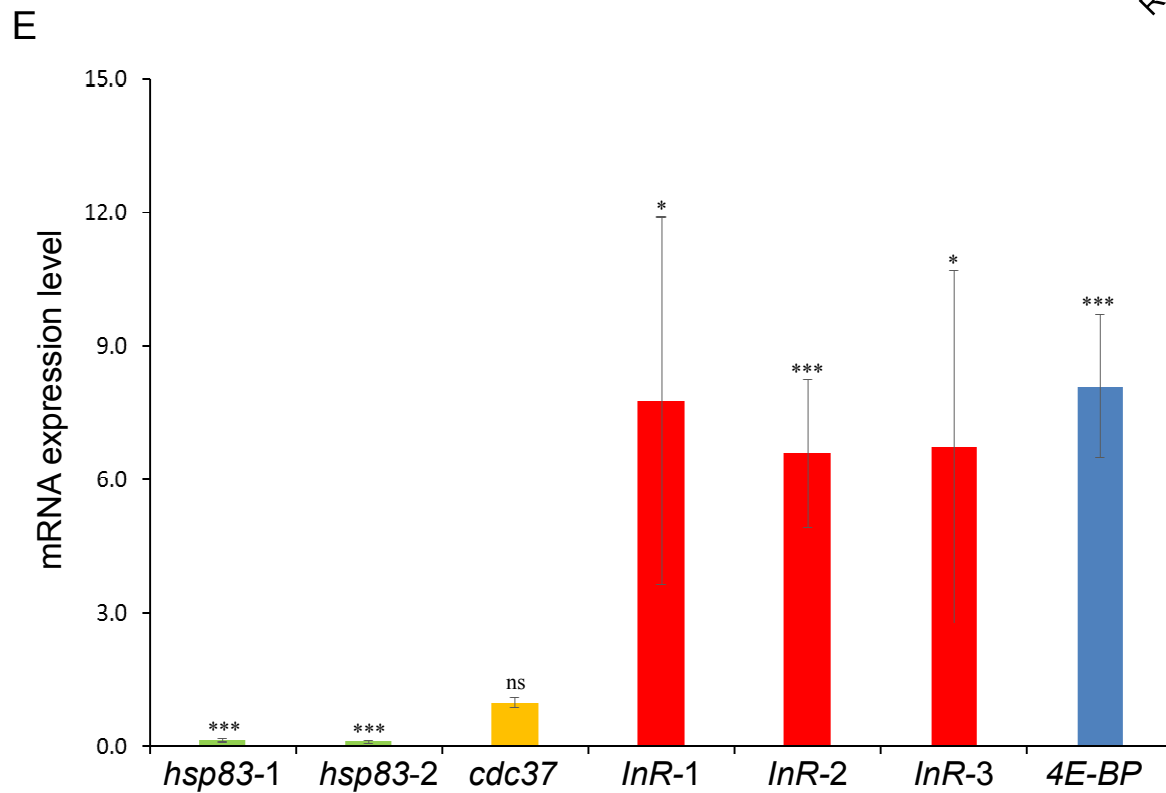
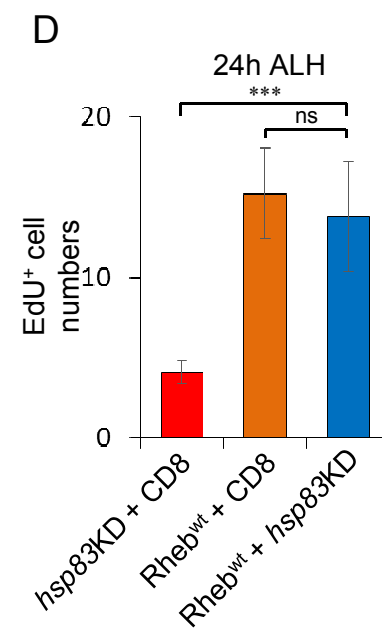
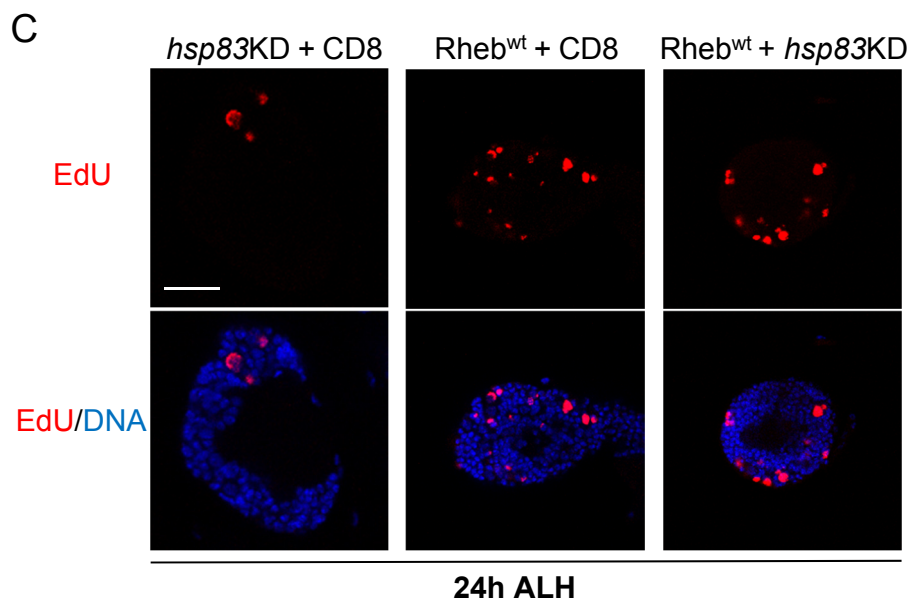
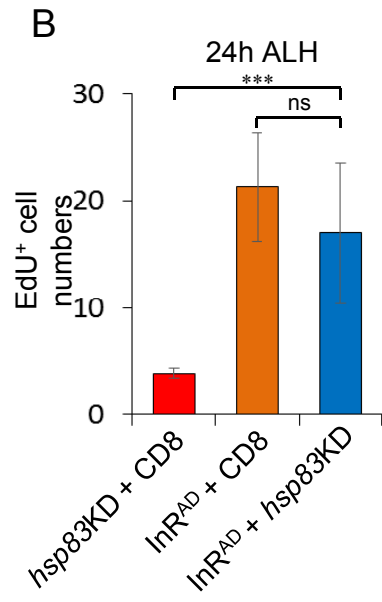
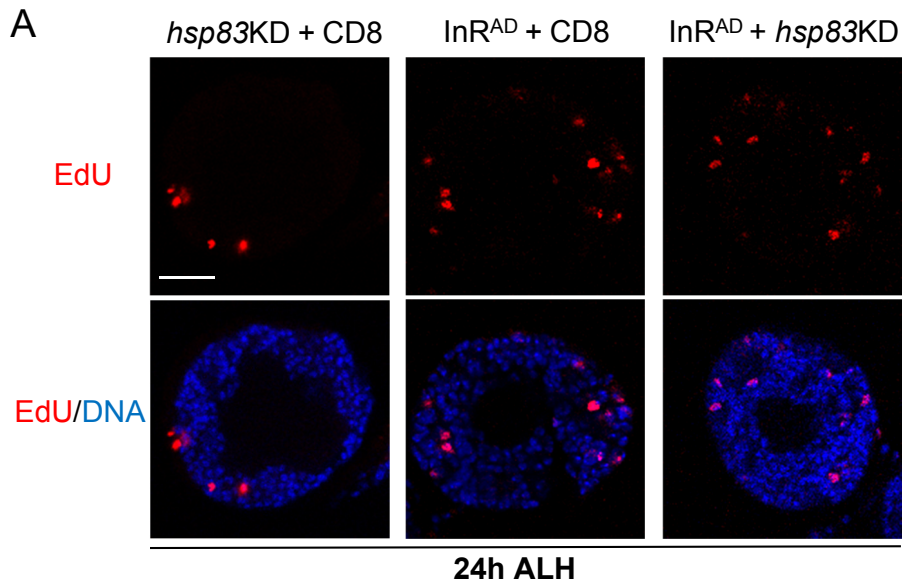


Figure S5. Hsp83 functions upstream of InR/PI3K/Akt pathway during NSC reactivation

(A, B) Larval brains overexpressing *InR^{AD}* (BDSC#8440) with *hsp83* knockdown (VDRC#108568) under *insc-Gal4* at 24h ALH in sucrose-only food were labeled with EdU (red) and DNA (blue). The control used was *InR^{AD}* overexpression with UAS-CD8-GFP. Quantifications are presented in (B) as mean \pm SD. *hsp83* knockdown, 3.9 ± 0.5 (n=14) EdU⁺ cells per brain hemisphere at 24h ALH. Statistical analyses were done comparing between *InR^{AD}* overexpression and *InR^{AD}* overexpression with *hsp83* knockdown using two-tailed Student's *t*-test. ns: non-significant. Scale bars, 15 μ m. (C, D) Larval brains overexpressing *Rheb^{wt}* (BDSC#9689) with *hsp83* knockdown (VDRC#108568) or with UAS-CD8-GFP (control) under *insc-Gal4* at 24h ALH in sucrose-only food were labeled with EdU (red) and DNA (blue). Data are presented in (D) as mean \pm SD. *hsp83* knockdown, 4.1 ± 0.7 (n=13) EdU⁺ cells per brain hemisphere at 24h ALH. Statistical analyses were done comparing between *Rheb^{wt}* overexpression and *Rheb^{wt}* overexpression with *hsp83* knockdown using two-tailed Student's *t*-test. ns: non-significant. Scale bars, 15 μ m. (E) qPCR analysis of *hsp83*, *cdc37*, *InR* and *4EBP* in whole larvae of control (*yellow-white*, *yw*, fed with normal food) and nutritional restricted condition (*yw* in sucrose-only) at 24h ALH. The mRNA levels of *hsp83* were accessed by two different pairs of primers, while *InR* mRNA level were measured by three different pairs of primers. In sucrose food, the mRNA level of *cdc37* changes to $97.3\% \pm 10.6\%$ (n=4) compared to control, while the mRNA level of *4E-BP* was $808.7\% \pm 161.8\%$ (n=4). Three different pairs of primers showed the mRNA levels of *InR* were $776.3\% \pm 413.5\%$ (n=4), $658.8\% \pm 167.3\%$ (n=4) and $673.7\% \pm 395.4\%$ (n=4) respectively compared with control. Statistical analyses were done comparing between control (actin5C, GADPH1, GADPH2, G6DPH and RPII215) and nutritional restricted condition, using two-tailed Student's *t*-test. The mRNA levels of control were normalized to 1. ns: non-significant; **P*<0.05; ****P* < 0.001.

SUPPLEMENTAL EXPERIMENTAL PROCEDURES

Immunocytochemistry

Larval brains were dissected in phosphate-buffered saline (PBS) and fixed for 22 minutes in 0.3% PBS-Triton (PBT) with 4% EM grade formaldehyde (methanol-free). Fixed brains were then washed three times with 0.3% PBT for 10 minutes each. After washing, brains were blocked with 3% bovine serum albumin (BSA) in 0.3% PBT for 45 minutes and then incubated with primary antibody diluted in 3% BSA overnight at 4°C. Following two more washings (10 minutes each), larval brains were incubated with secondary antibody diluted in 0.3% PBT for 90 minutes. DNA was labelled by ToPro-3 (1:5000, Invitrogen, Cat#: T3605) or DAPI (1:1500, Molecular Probes, Cat#: D1306). Larval brains were mounted in Vector shield (Vector Laboratory) for Confocal microscopy. Samples were analyzed with a Zeiss LSM710 Confocal microscope and processed with Adobe Photoshop CS6.

Primary antibodies used were: guinea pig anti-Dpn (1:1000, J Skeath), rat anti-CD8 (1:250, Invitrogen, Cat#: MCD0800), rabbit anti-GFP (1:500, Molecular Probes, Cat#: A21311), mouse anti-Mira (1:40, F. Matsuzaki), mouse anti-Dac (1:5, DSHB, Cat#: mAbdac2-3), rabbit anti-Akt (1:100; Cell signaling, Cat#: 4691), mouse anti-Myc (1:200, abcam, Cat#: ab32) and rabbit anti-HA (1:100, Sigma, Cat#: H6908).

EdU pulse-chase analysis

Larvae were fed with standard food supplemented with 0.2mM EdU from *Click-iT*® EdU Alexa Fluor® 555 *Imaging Kit* (Invitrogen) for 4 hours prior to dissection. The dissected larval brains were then fixed with 4% EM grade formaldehyde (in 0.3% PBT) for 22 minutes. The brains were washed three times and blocked with 3% BSA in PBT for 1 hour. Following blocking, EdU was detected by Alexa Fluor azide according to the *Click-iT* EdU protocol (Invitrogen). The brains were then washed twice and blocked with 3% BSA again for 30 minutes, and processed by immunohistochemistry.

Deprivation of dietary amino acids in larvae

To deprive larvae of dietary amino acids, larvae were transferred to 5% sucrose, 1% Agar in PBS within 2 hours after larval hatching. Larvae were raised at appropriate temperature at various time points prior to further analysis.

Quantification of cellular extensions and EdU incorporation

Following immunostaining, *Drosophila* larval brains were placed on microscope slides with their dorsal side up. The confocal z-stacks were taken from the dorsal surface to the deep layers of the larval brains (24-30 slides per z-stack with 3 μm intervals). Quantification was carried out using ImageJ or Zen software.

Generation of plasmids and transgenic flies

Plasmid constructs were generated using Gateway® BP Clonase® II Enzyme mix (Invitrogen). cDNA clones used in this study were AT20544 (*hsp83*) and FI07667 (*cdc37*) (Drosophila Genomics Resource Centre [DGRC]). pENTR-InR containing the full length of InR cDNA was kindly provided by Dr. H. Stocker. InR^{intra} domain was referred from Dr. H. Stocker's published research (Almudi et al., 2013). Hsp83C contains only the C-terminal domain of Hsp83, from amino acid 538-717. Briefly, desired regions of genes were amplified by polymerase chain reaction (PCR) and inserted into a Gateway entry vector pDONR221 (Invitrogen) using Gateway BP Clonase II Enzyme mix. They were subsequently inserted into Gateway destination vectors (PAMW, PAHW, pUAST-CYFP-HA-RfB, pUAST-NYFP-Myc-RfB, pUAST-RfB-HA-CYFP and pUAST-RfB-Myc-NYFP) by LR recombination using Gateway LR Clonase II enzyme mix. Primers used for generating entry clones were listed in Table S2.

Gateway destination vectors pUAST-CYFP-HA-RfB (RfB, reading frame cassette B, a Gateway recombination cassette for LR recombination), pUAST-NYFP-Myc-RfB, pUAST-RfB-HA-CYFP and pUAST-RfB-Myc-NYFP were kindly provided by Dr S. Bogdan. To remove the Gateway recombination cassettes that contains multiple STOP codons and allow the expression of half-YFP in the control vectors, 2xHA and 3xMyc sequence were inserted into pDONR221 to generate Gateway entry clones pDONR221-2xHA and pDONR221-3xMyc respectively. Next, 2xHA and 3xMyc from entry clones were inserted into destination vectors pUAST-RfB-HA-CYFP and pUAST-RfB-Myc-NYFP respectively to generate C-terminal tagging control plasmids pUAST-HA-CYFP and pUAST-Myc-NYFP (primers listed in Table S2). For N-terminal tagging controls, a 99base pair sequence containing multiple stop codons was inserted (Koe C., unpublished data; Table S2) into destination vectors to remove Gateway recombination cassettes. Sequences inserted were:

GCTGAAACGAAGTTAACTTTGAGGTGTACGGGTAAGTATTAGAAAGCAGGACTAAACGACCATA

TCCTCATGTCGTCGGCCGCGGACCATTGAATAG.

In brief, the sequences were inserted into pDONR211 to generate entry clones first (Modifier pDONR211) and then cloned into destination vectors PAMW, PAHW, pUAST-CYFP-HA-RfB and pUAST-NYFP-Myc-RfB. The plasmids generated were N-terminal tag control Myc (PAMW-*actin5C*-6xMyc), HA (PAHW-*actin5C*-3xHA), pUAST-CYFP-HA and pUAST-NYFP-Myc. To generate tagged constructs of Hsp83, Hsp83C, Cdc37, and InR^{intra}, the following entry clones were generated pDONR211-Hsp83, pDONR211-Cdc37, pDONR-InR^{intra} (with or without stop codon), and pDONR211-Hsp83C (without stop codon). Next, cDNA from entry clones was inserted into destination vectors (PAMW, PAHW, pUAST-RfB-HA-CYFP, and pUAST-RfB-Myc-NYFP). The plasmids generated were pUAST-Hsp83-Myc-NYFP, pUAST-Hsp83-HA-CYFP, pUAST-Hsp83C-Myc-NYFP, pUAST-Cdc37-Myc-NYFP, pUAST-Cdc37-HA-CYFP, pUAST-InR^{intra}-HA-CYFP, Myc-Hsp83, HA-Hsp83, Myc-Cdc37 and HA-InR^{intra}.

UAS-CYFP-HA, UAS-NYFP-Myc, UAS-Hsp83-Myc-NYFP, UAS-Cdc37-Myc-NYFP, UAS-Cdc37-HA-CYFP and UAS-InR^{intra}-HA-CYFP were generated by Φ C31-integrase system by BestGene, Inc. The stocks injected were BDSC#8622 yw; P{y[+t7.7]=CaryP}attP2 (chromosome III, 68A4).

***Drosophila* Hsp83 domain analysis**

Full length of amino acid sequence of Hsp83 was obtained from Flybase and analyzed by Simple Modular Architecture Research Tool (SMART).

***Drosophila* genomic constructs and genomic rescue**

Bacterial artificial chromosomes (BACs), CH322-129N17 for *hsp83* and CH322-35F18 for *cdc37*, covering from 10,000 bp upstream to 5,000 bp downstream of the genomic region of the genes, were obtained from the BACPAC Resources Center. Transgenic flies expressing the BAC clone were generated by Φ C31-integrase system by BestGene, Inc. The stocks injected were BDSC#8621 yw; P{y[+t7.7]=CaryP}attP1 (chromosome II, 55C4).

S2 cell culture and transient transfection

Drosophila S2 cells were cultured in Express Five serum free medium (Gibco), and supplemented with 2mM glutamine (Thermo Fisher Scientific). For *in vitro* bimolecular fluorescence complementation (BiFC), 1×10^6 cells S2 cells were seeded directly to Poly-L-lysine (PLL)-coated cover slips (Iwaki). For PLA assay, 5×10^4 cells were seeded to 8-well chamber slides (Lab-Tek, Cat#: 154941). Plasmids were transfected into S2 cells together using Effectene Transfection Reagent (QIAGEN). For *in vitro* bimolecular fluorescence complementation (BiFC), S2 cells were transfected with *actinC5*-Gal4 and the respectively BiFC constructs each at 200 ng per well. For PLA, the transfection amount for each plasmid is 50 ng.

Bimolecular fluorescence complementation (BiFC)

For *in vitro* BiFC, the expression of BiFC constructs was under the control of *actinC5*-Gal4, which was co-transfected with the plasmids. Coverslips coated with S2 cells were collected after 48 hours of transfection, S2 cells were rinsed with PBS and fixed with 4% EM-grade formaldehyde in 0.1% PBS-Triton (PBT) for 15 minutes followed by three rinses with 0.1% PBT. Fixed cells were blocked with 5% BSA (in 0.1% PBT) for 1 hour and incubated with primary antibodies diluted in 5% BSA for 2 hours at room temperature. Antibodies used for BiFC were mouse anti-Myc (1:2000, abcam, Cat#: ab32) and rabbit anti-HA (1:2000, Sigma, Cat#: H6908). Cells were then rinsed twice with 0.1% PBT and incubated with secondary antibody diluted in 0.1% PBT for 1 hour. Cells were rinsed with 0.1% PBT again for two times. Coverslips were then mounted onto glass slides using Vector shield (Vector Laboratory) for Confocal microscopy. pUAST-HA-CYFP, pUAST-Myc-NYFP, pUAST-Hsp83-Myc-NYFP, pUAST-Hsp83-HA-CYFP, pUAST-Hsp83C-Myc-NYFP, pUAST-Cdc37-Myc-NYFP, pUAST-InR^{intra}-HA-CYFP and pUAST-WAVE-HA-CYFP (Bogdan, S) were used for *in vitro* bimolecular fluorescence complementation (BiFC). For *in vivo* BiFC, the constructs were expressed under *insc*-Gal4 and followed by standard immunohistochemistry.

Proximity ligation assay (PLA)

The basis of PLA is as follows: primary antibodies bind to tagged proteins of interest are recognized by secondary antibodies conjugated with PLA probe PLUS and PLA probe MINUS; if two proteins of interest are present in close proximity (<40 nm), the connector oligos hybridize to PLA probes and are ligated by T4 ligases. Ligated oligos form a circular template and can be amplified with DNA polymerase. Amplified DNA is bound by

fluorescent-labeled complementary oligos, resulting fluorescent spots *in situ*. For proximity ligation assay (PLA), plasmids used were control Myc (PAMW-*actin5C*-6xMyc), control HA (PAHW-*actin5C*-3xHA), Myc-Hsp83, HA-Hsp83, Myc-Cdc37, HA-InR^{intra} and Myc-Akt (Li et al., 2014).

After 48 hours of transfection, chamber slides with S2 cells were rinsed with cold PBS three times and fixed with 4% EM-grade formaldehyde in PBS for 15 minutes. Cells were rinsed with cold PBS three times (2 minutes each time), blocked with 5% BSA (in 0.1% PBT) for 1 hour and incubated with primary antibodies diluted in 5% BSA (in 0.1% PBT) for 2 hours. Cells were then incubated with PLA probes followed by ligation and amplification according to manufacturer's protocol (Sigma-Aldrich). Cells were then incubated with the same primary antibodies again for 2 hours (diluted in 5% BSA in PBS). After rinses with PBS once, cells were incubated with secondary antibody diluted in PBS for 90 minutes. Cells were mounted in *in situ* Mounting Medium with DAPI (Sigma-Aldrich) for Confocal microscopy.

Protein extraction and immunoblotting

Larval brains dissected in PBS or whole larvae at 6h ALH were homogenized in RIPA buffer (50 mM Tris pH7.5, 150 mM NaCl, 1 mM EDTA, 1% TritonX-100, 0.5% sodium deoxycholate, 0.1% SDS). Proteins were separated by SDS-PAGE and analyzed by western blotting.

Blots were probed with the following antibodies: mouse anti-Actin (1:5000; MP Biomedicals, Cat#: 08691001), rabbit anti-Akt (1:1500; Cell signaling, Cat#: 4691), rat anti-Hsp83 (1:1000; Abcam, Cat#: 13492) and rabbit anti-pInR (1:1000; Cell signaling, Cat#: 3021).

RNA extraction and qPCR analysis

RNA from larval brains or whole larvae was extracted using TRI reagent (Sigma-Aldrich) following the manufacturer's protocol. Reverse transcription was carried out using ProtoScript First Strand cDNA Synthesis kit (New England Biolabs, Inc.).

qPCR was performed using SsoFast™ EvaGreen® supermix (Bio-Rad) with different primer pairs. Primers were picked using Primer3 with default setting, except the following: Hsp83-2 (Sawarkar et al., 2012), InR-2 (Danielsen et al., 2014) and 4E-BP (Owusu-Ansah et al., 2013). The primers used were listed in Table S3.

The experiments were ran using Bio-Rad CFX96™ Real-Time PCR system. Program used was: 95°C for 3 second, 56°C for 30 second and plate read for 40 cycles. Melt curve: 65°C - 95°C with 0.5°C increment for 5 second followed with plate read. Results were analyzed using REST excel file.

Statistical analysis

Statistical analysis among different groups was performed by two-tailed unpaired Student's t-test, and a value of $P < 0.05$ was considered as statistical significant. In this work, ns (non-significant) indicates $P > 0.05$, * indicates $P < 0.05$, ** indicates $P < 0.01$ and *** indicates $P < 0.001$. All quantification data were shown as mean \pm SD, except for MARCM clones that only percentages were calculated.

SUPPLEMENTAL REFERENCES

- Almudi, I., Poernbacher, I., Hafen, E., and Stocker, H. (2013). The Lnk/SH2B adaptor provides a fail-safe mechanism to establish the Insulin receptor-Chico interaction. *Cell communication and signaling : CCS* *11*, 26.
- Danielsen, E.T., Moeller, M.E., Dorry, E., Komura-Kawa, T., Fujimoto, Y., Troelsen, J.T., Herder, R., O'Connor, M.B., Niwa, R., and Rewitz, K.F. (2014). Transcriptional control of steroid biosynthesis genes in the *Drosophila* prothoracic gland by ventral veins lacking and knirps. *PLoS genetics* *10*, e1004343.
- Li, S., Wang, C., Sandanaraj, E., Aw, S.S., Koe, C.T., Wong, J.J., Yu, F., Ang, B.T., Tang, C., and Wang, H. (2014). The SCFSlimb E3 ligase complex regulates asymmetric division to inhibit neuroblast overgrowth. *EMBO reports* *15*, 165-174.
- Owusu-Ansah, E., Song, W., and Perrimon, N. (2013). Muscle mitohormesis promotes longevity via systemic repression of insulin signaling. *Cell* *155*, 699-712.
- Sawarkar, R., Sievers, C., and Paro, R. (2012). Hsp90 globally targets paused RNA polymerase to regulate gene expression in response to environmental stimuli. *Cell* *149*, 807-818.